



HAL
open science

Incorporation of calcium in glasses: a key to understand the vitrification of sewage sludge

Mariona Tarrago, Irene Royo, Maite Garcia- Valles, Salvador Martinez, Daniel R Neuville

► **To cite this version:**

Mariona Tarrago, Irene Royo, Maite Garcia- Valles, Salvador Martinez, Daniel R Neuville. Incorporation of calcium in glasses: a key to understand the vitrification of sewage sludge. International Journal of Applied Glass Science, 2021, 10.1111/ijag.15920 . hal-03208408

HAL Id: hal-03208408

<https://univ-angers.hal.science/hal-03208408>

Submitted on 26 Apr 2021

HAL is a multi-disciplinary open access archive for the deposit and dissemination of scientific research documents, whether they are published or not. The documents may come from teaching and research institutions in France or abroad, or from public or private research centers.

L'archive ouverte pluridisciplinaire **HAL**, est destinée au dépôt et à la diffusion de documents scientifiques de niveau recherche, publiés ou non, émanant des établissements d'enseignement et de recherche français ou étrangers, des laboratoires publics ou privés.

Manuscript Number:

Title: Incorporation of calcium in basaltic glasses: a key to understand the vitrification of sewage sludge

Article Type: Full length article

Keywords: glass-ceramic, sewage sludge, calcium, valorization, viscosity, nucleation

Corresponding Author: Dr. Mariona Tarrago, Ph.D.

Corresponding Author's Institution: Institut de Physique du Globe de Paris

First Author: Mariona Tarrago, PhD

Order of Authors: Mariona Tarrago, PhD; Irene Royo, B.Sc.; Maite Garcia-Valles, Ph.D.; Salvador Martinez, Ph.D.; Daniel R. Neuville, Ph.D.

Abstract: The quantity of sewage sludge generated daily in water decontamination represents a major environmental problem. Remediation strategies focus on using the wastes as raw materials to reduce storage costs and minimize the need for mining. An approach by vitrification reduces the volume of waste and inertizes hazardous elements by binding them to the structure of chemically stable glasses and glass-ceramics. The valorization process of sewage sludge by vitrification has been simulated by producing a glass and a glass-ceramic from a basalt enriched in calcium that lies between the stability fields of pyroxene and melilite in the system CaO-MgO-SiO₂-Al₂O₃. Nucleation at the temperature of maximum nucleation rates (650 and 675 °C) of this glass causes the formation of a biphasic system (crystal + glass) that constrains its rheological behavior enhancing the formation of a large amount of nuclei that result in a fine microstructure, forming a glass-ceramic. The microhardness of the glass (8.2 GPa) and the glass-ceramic (8.6 GPa) and leaching tests (in the ppb range) place both the glass and the glass-ceramics at the high end of the mechanical properties and chemical resistance of ceramic tiles for the building industry.

Suggested Reviewers: Alexander Karamanov PhD
Professor, Department of Phase Formation, Crystalline and Amorphous Materials, Bulgarian Academy of Sciences
karama@ipc.bas.bg

Prof. Karamanov is a world-class expert in the vitrification of wastes and has extensively worked in the production process of glass-ceramics.

Ina Mitra PhD
Senior Scientist, Schott AG
ina.mitra@schott.de

Dr. Ina Mitra is a Senior Scientist at the glass producer Schott AG (Germany), where she develops glasses and glass-ceramics for devices in industrial applications.

Pura Alfonso PhD

Professor, Mining Engineering and Natural Resources, Universitat

Politècnica de Catalunya

pura@emrn.upc.edu

Prof. Alfonso has extensively worked in vitrification and glass-ceramics production as a means to give a new use to mining waste.

Opposed Reviewers:



Mariona TARRAGÓ
Géomatériaux
Institut de physique du globe de Paris
UMR 7154
+ 33 (0)1 83 95 7758
tarrago@ipgp.fr

**Editor, Ceramics
International**

Submission to Ceramics International

Paris
11th of March 2020

Dear Editor,

Please find enclosed our manuscript "Incorporation of calcium in basaltic glasses: a key to understand the vitrification of sewage sludge" by M. Tarragó, I. Royo, M. Garcia-Valles, S. Martínez and D.R. Neuville, which we would like to submit for publication as a peer-reviewed Article in the Ceramics International.

This manuscript brings new data on the inertization and valorization of sewage sludge simulated using a Ca-enriched basalt. The nucleation and crystal growth temperatures of all the phases have been carefully investigated in order to obtain a glass-ceramic with superior physicochemical properties than the parent glass. Our data on the stability of merwinite confirms its crystallization as a metastable phase.

We think our findings would appeal to the readership of the Ceramics International as vitrification is a means of reducing the storage issues and chemical hazards related to the landfilling of wastes. The results show potential of sewage sludge-like materials as inertization matrix for industrial wastes containing potentially toxic elements such as tannery (Cr) or galvanic sludge (Cu, Zn). The obtained glasses and glassceramics can be used as abrasion-resistant materials in construction.

We would like to suggest, if the Editor finds it appropriate, Prof. Alexander Karamanov, Dr. Ina Mitra, and Prof. Pura Alfonso as reviewers of our work. They all have extensive research experience in glass and crystallization processes in wastes.

This manuscript has not been published elsewhere nor is under consideration by another journal. All authors approve the manuscript and agree with its submission to the Ceramics International.

We are looking forward to receiving your decision about our work.

Yours sincerely,

Mariona Tarragó

Signature

Incorporation of calcium in basaltic glasses: a key to understand the vitrification of sewage sludge

M.Tarrago^{1,2*}, I. Royo¹, S. Martínez¹, M. Garcia-Valles¹ and D.R. Neuville²

¹Dpt., Mineralogia, Petrologia i Geologia Aplicada, Fac. de Ciències de la Terra. Universitat de Barcelona, c/ Martí i Franquès, s/n, 08028 Barcelona (Spain)

²Géomatériaux, CNRS-Institut de Physique du Globe de Paris, Université de Paris, 1 rue Jussieu 75005 Paris (France)

E-mail tarrago@ipgp.fr

*Corresponding author

Abstract

The quantity of sewage sludge generated daily in water decontamination represents a major environmental problem. Remediation strategies focus on using the wastes as raw materials to reduce storage costs and minimize the need for mining. An approach by vitrification reduces the volume of waste and inertizes hazardous elements by binding them to the structure of chemically stable glasses and glass-ceramics. The valorization process of sewage sludge by vitrification has been simulated by producing a glass and a glass-ceramic from a basalt enriched in calcium that lies between the stability fields of pyroxene and melilite in the system CaO-MgO-SiO₂-Al₂O₃. Nucleation at the temperature of maximum nucleation rates (650 and 675 °C) of this glass causes the formation of a biphasic system (crystal + glass) that constrains its rheological behavior enhancing the formation of a large amount of nuclei that result in a fine microstructure, forming a glass-ceramic. The microhardness of the glass (8.2 GPa) and the glass-ceramic (8.6 GPa) and leaching tests (in the ppb range) place both the glass and the glass-ceramics at the high end of the mechanical properties and chemical resistance of ceramic tiles for the building industry.

Keywords: glass-ceramic, sewage sludge, calcium, valorization, viscosity, nucleation

1. Introduction

1 Decontamination processes of wastewater daily generate huge volumes of sewage sludge, the solid
2 fraction separated the treatment (including domestic septage) [1]. In Catalonia (population 7.5 M),
3
4 water processing produced 119,230 tons of dry sewage sludge in 2015 [2]. The production of sludge
5
6 peaked on the 2004–2008 period, averaging 140,000 tons per year [2] and decreased in a context of
7
8 economic crisis that is currently receding. The disposal of these sewage sludge concerns two
9
10 economically relevant issues: the availability of storage space in landfills and the environmental
11
12 pollution that may derive from the sludge composition. An approach to solve this problem consists
13
14 in designing new products using sewage sludge as a raw material – such as glasses and glass-
15
16 ceramics for structural uses in the construction industry.
17
18

19
20 The preferred disposal of sewage sludge is its application in agricultural lands. However, this
21
22 solution is limited to sludge that comply with the increasingly restrictive regulations established by
23
24 the environmental governing bodies. Sewage sludge may contain concentrations of potentially toxic
25
26 elements (PTE) that exceed by at least an order of magnitude those established by the European
27
28 Economic Community for agricultural application [3], and Table 1. Hence, the design of new,
29
30 environmentally safe products is crucial to optimize waste disposal processes. Vitrification is a
31
32 valorization alternative where sewage sludge may be used as a raw material to produce glass
33
34 appropriate for the building industry in the form of wall tiles or pavements [4]. Its advantages lie on
35
36 both reducing the volume of the waste and binding of the components of the sludge – including the
37
38 PTE – in the glass structure. Further inertization can be achieved using a glass-ceramic process,
39
40 where the PTE will be emplaced in newly-formed mineral phases [5,6]. An inertization matrix
41
42 analogous to sewage sludge may, once proven effective, be tested to bind industrial wastes such as
43
44 galvanic or chromium sludge, which contain large concentrations of Zn and Ni, and Cr respectively.
45
46 Any potential applications are constrained by the bulk composition of sewage sludge, which largely
47
48 depends on its source area. Factors such as urban/rural origin, the actual processing undertaken at
49
50 the wastewater treatment plant, seasonal variations related to changes in upstream activity or in
51
52
53
54
55
56
57
58
59
60
61
62
63
64
65

microbial activity [7,8], long-term changes of soil uses of the watershed area, or the degree of groundwater contamination [9] influence the variability and the final composition of the sludge. The average composition of the inorganic fraction of urban sewage sludge (USS) may be simulated using basalt [4,10–16] and Table 1), the main differences being the concentration of Ca, Mg and P. The addition of P to the basalt develops an increasingly sharp phase separation in the glass that results in partial crystallization, increasing the microhardness of the final products [17]. The addition of Ca is expected to improve the properties of the basalt glass by increasing microhardness and reducing viscosity.

Table 1. Composition of the basalt from Sant Joan les Fonts (measured using X-Ray fluorescence) compared to analyses of sewage sludge from WWTP reported on the literature [4,10–16]. The asterisks correspond to the values which exceed the range of real sludge compositions. The maximum concentrations are reported for the trace elements.

Oxide	Basalt	USS compositions
Major components (wt%)		
SiO ₂	43.98	33 - 53.14
CaO	10.11	7.7 - 37.67
Al ₂ O ₃	14.16	11.73 - 21.48
FeO	10.88	4.64 - 10
MgO	10.05*	2.4 - 6.52
Na ₂ O	3.31	0.6 - 5.2
TiO ₂	2.51	1.19 - 2.9
K ₂ O	1.98	0.9 - 3.8
P ₂ O ₅	0.55*	2.62 - 5.2
MnO	0.17	0.12 - 0.44
Trace elements (ppm)		
Ba	585.4	330
Cr	263.5	1268
Cu	63.6	12701
Ni	172.9	1025
Pb	4.9	3519
Zn	86.2	31166

The properties of a successfully vitrified waste may be improved by a glass-ceramic process. A glass-ceramic is any material produced from (partially) crystallized glass [18,19]. The strengths of glass-ceramics as performing materials arise from their unique microstructure, achieved from the understanding of the nucleation and crystallization processes. Controlling the composition of the

parent glass, the nucleation and crystallization processes and their effect on the rheological behavior is also essential to achieve low viscosity at high temperature, and to optimize the resistance to abrasion and chemical alteration [5,6]. Other interesting properties of glass-ceramics regarding their stability are the lack of porosity and high strength and toughness [18]. Ca-rich wastes are good candidates for vitrification and subsequent glass-ceramic processing - in products such as Sital slag from the steel and copper industries of Russia [20], cupola slag blast [21], blast furnace slag [22], tin tailings [23], molybdenum tailings [24], and tungsten tailings [25,26].

Xu and coworkers [27] studied the evolution of the nucleation rate on $\text{Na}_2\text{O}-2\text{CaO}-3\text{SiO}_2$ glass and produced a glass-ceramic with fine-grained (crystal diameter about 10 μm), homogenous glass. Their approach determined the temperatures of maximum nucleation rate using thermal analysis to establish the appropriate production procedure. The present study applies this method to the measurement of the temperatures of maximum nucleation rate of multiple phases on a glass representing a simplified composition of sewage sludge to produce a glass-ceramic with enhanced mechanical properties and chemical durability.

2. Material and methods

2.1. Glass synthesis

The production process of the parent glass (original composition) consists of mixing 84 wt% basalt from Boscarró old quarry (Sant Joan les Fonts, SJLFB, Catalunya) (Table 1) with 23 wt% reagent grade CaCO_3 (Panreac 121212) to provide the additional Ca. This composition should lie in the suitable workability range due to Ca's expected decrease effect on the melting point of basalt [12].

The mixture is homogenized by crushing in a ball mill and then melted in a Pt crucible in a globular alumina furnace equipped with SuperKanthal® heating elements. The melting process consisted of heating the batch at 2 °C/min up to 1000 °C, followed by an isothermal step during 30 minutes to complete decarbonation and further heating at 1 °C/min up to 1450 °C followed by an isothermal step during 4h. The melt is then quenched by pouring on a copper plate. The melting-crushing cycle

is repeated twice to ensure homogenization. The whole batch made about 200 g of the parent glass.

Part of the glass is then annealed in a TechnoPiro® muffle furnace preheated at 500 °C for 24 h to be able to cut a prism for the dilatometry measurements. No significant weight loss occurred during the production process.

2.2. Glass-ceramic production

The thermal treatment of the parent glass to obtain the glass-ceramic included the following steps based on the temperatures of maximum nucleation rate (T_{MNR}) determined during the study:

- Heating up to 650 °C at 2 °C/min for 6 h (T_{MNR} of magnetite)
- Heating at 675 °C at 2 °C/min for 6 h (2nd T_{MNR} , discussed further in the manuscript)
- Heating up to 874 °C at 10 °C/min for 6 (the temperature of the exothermic DTA peak)
- Heating to 1000 °C at 2 °C/min for 6 h (at this temperature merwinite has been exhausted by reacting with diopside to form akermanite)
- Free cooling

2.3. Chemical composition

The chemical composition of the basalt has been measured by X-Ray Fluorescence using a sequential X-ray spectrophotometer Phillips PW2400. The major elements have been measured in lithium tetraborate pearls and the trace elements in pressed pellets.

The chemical composition of the parent glass has been measured in a JEOL JXA 8230 electron microprobe (EMPA). Quantitative electron microprobe analyses have been obtained in wavelength-dispersive spectroscopy (WDS) mode, operating with an accelerating voltage of 20 kV, a beam current of 16 nA for Al, Si, Ti, Ca, K, Mg, Fe, Mn, 8nA for Na and 6 nA for P, and a beam diameter of 5 μm. Corundum ($AlK\alpha$), wollastonite ($SiK\alpha$, $CaK\alpha$), rutile ($TiK\alpha$), orthoclase ($KK\alpha$), apatite ($PK\alpha$), periclase ($MgK\alpha$), albite ($NaK\alpha$), synthetic Fe_2O_3 ($FeK\alpha$) and rhodonite ($MnK\alpha$) have been used as standards. The employed analyzing crystals have been TAP for Al and Si, PETJ for Ti, Ca, K and P, TAPH for Mg and Na and LIFH for Fe and Mn.

2.4. Raman spectroscopy

The Raman spectrum of the parent glass has been obtained with a T64000 Jobin-Yvon Raman spectrometer equipped with a CCD detector. The light source was an Ar⁺ ion laser operating at 488 nm with a typical output of 100 mW on the sample. The integration time was 900 s and the spectral range was between 100 – 1500 cm⁻¹. The spectrum has been treated with the Long correction (Long, 1977, Neuville and Mysen, 1996) and normalized to the total area [29,30].

2.5. Thermal analysis

Glass thermal evolution has been studied by Differential Thermal Analysis (DTA) in a Netzsch DTA-TG STA 409C equipment. A preliminary analysis is made on glass powder (particle size <50 μm) at 10 °C/min in an alumina crucible under a 70 mL/min N₂ flow and using pure Al₂O₃ (Perkin-Elmer 0419-0197) as a reference material to determine the crystallization events. The small particle size ensures full crystallization of the sample. The rest of the as-quenched glass is then ground and screened to a particle size between 400 and 500 μm to ensure bulk crystallization. Further DTA measurements are performed using about 70 mg of glass sample.

The glass particles are heated at 15 °C/min up to nucleation temperatures (T_N) between 500 – 850 °C during 3 h and then further heated up to 1350 °C before cooling. These treatments to different T_N cause a shift of the temperature of the exothermic DTA peak attributed to crystallization. The temperature of the maximum nucleation rate is then determined from the plot of the inverse of the temperature of the exothermic peak as a function of the nucleation temperature [27].

2.6. X-Ray diffraction

The presence of amorphous and crystalline phases in the glass and after thermal treatments is assessed by X-Ray Diffraction (XRD) obtained in a PANalytical X'Pert PRO MPD Alpha1 powder diffractometer in Bragg-Brentano $\theta/2\theta$ geometry (radius of 240 millimetres, Cu K α 1 radiation ($\lambda =$

1.5406 Å), work power 45 kV – 40 mA, scanning range 4 – 80° 2θ with step size of 0.017° and measuring time 50 s. In-situ X-Ray Diffraction (XRD) under vacuum atmosphere was carried out in an Anton Paar HTK1200N High Temperature chamber (HT-XRD) coupled to the previously described equipment. The experiment consisted in heating powdered glass at a rate of 20 °C/min with 1h isothermal steps at 28, 300, 500, then from 550 to 1200 °C, and 28 °C after cooling – 7 spectra were taken during each one of these steps. Data from the HT-XRD patterns were used to determine how the intensity of certain peaks varies with temperature as well as to calculate the coherent size of the crystallites of each mineral phase nucleated during the thermal treatment from Scherrer's equation (Eq. 1) [31]:

$$\tau = \frac{K\lambda}{\beta \cos\theta} \quad [\text{Eq 1}]$$

In this equation τ stands for the average size of the crystalline domains; K is a dimensionless shape (0.9), λ is the X-Ray wavelength (1.5406); β is the full width of the peak at half maximum minus the instrumental line broadening, in radians; and θ is the Bragg angle – in radians.

The quantification of the mineral phases of the glass-ceramic was obtained from the Rietveld refinement of the XRD non-oriented powder diffraction on FullProf v 3.00 software [32].

2.7. Dilatometry

The dilatometric curve of the glass is obtained in a Linseis L76/1550 horizontal dilatometer at a heating rate of 10 °C/min and air flow of 5 mL/min. The glass transition temperature (T_g) is calculated from the curve using the tangents method. The coefficient of thermal expansion is calculated between 100 and 500 °C.

2.8. Viscosity measurements

The effect of nucleation on the viscosity of glass is investigated by hot-stage microscopy (HSM) prototype [33]. The studied samples are nucleated at 650 °C in the DTA furnace according to the following sequence: the glass is heated at 10 °C/min up to 500 °C, where the temperature is

1 stabilized for 10 min and later increased at 20 °C/min up to the T_N for a period of time ranging from
2 0.5 to 8 h. The temperatures of the fixed viscosity points are then determined in glass powder
3 (diameter < 45 μm) cylinders produced in a uniaxial press using a 1/20 solution of Elvacite® in
4 acetone. The deformation of the probe during heating at 5 °C/min between 25 and 1450 °C is
5 recorded using the ProgRes CapturePro 2.8.8. software. The images corresponding to the fixed
6 viscosity points have been identified using Hot-Stage software [33]. The viscosity-temperature
7 curves have been plotted using the temperatures of the fixed viscosity points determined during the
8 HSM analysis and the viscosity values from Pascual and coworkers [34].
9
10
11
12
13
14
15
16
17
18
19

20 2.9. Electron microscopy

21 Textural information and qualitative punctual chemical analysis are obtained by scanning electron
22 microscopy (SEM) and Energy-Dispersive X-Ray Spectroscopy (EDX) using a JEOL J-7100 field
23 emission scanning electron microscope with EDS detector and backscattered electron detector
24 (BDS).
25
26
27
28
29
30
31
32
33
34

35 2.10. Microhardness Vickers

36 The Vickers hardness (VH) of the samples is measured on polished glass probes using a Galileo
37 Isoscan OD Vickers microindenter with a load of 294 N.
38
39
40
41
42
43
44

45 2.11. Leaching tests

46 Elementary analysis of the leachates serves to evaluate the stability of the glasses according to DIN
47 38414-S4 [35]. The test is performed in 10 g of sample – particle size between 2 and 4 mm – dried
48 at 50 °C and mixed in 100 mL of deionized water. The mixture is agitated at room temperature
49 during 24 h and the liquid is separated from the solid using a 0.45 μm pore size filter. The leachates
50 were analyzed by inductively coupled plasma optical emission spectrometry (ICP-OES, Optima
51
52
53
54
55
56
57
58
59
60
61
62
63
64
65

3100×, PerkinElmer) and inductively coupled plasma mass spectrometry (ICP-MS, Elan 6000, PerkinElmer).

3. Results

3.1. Original glass characterization

The chemical composition of the parent glass was elaborated from a basalt doped with calcium (Table 2). This mixture is comparable to USS compositions gathered from the literature – as explained in the introduction – in spite of some minor differences. It is enriched in Mg, and specially impoverished in P and Ca when compared to sludge [17,36]. The parent glass can be described as a calcic silicate with high Fe contents, which cause its dark brown color in thin section, black in bulk.

Table 2. Chemical composition of the parent glass B16Ca obtained by EMPA. The values in brackets correspond to the standard deviation of the measurements.

wt%	SiO ₂	Al ₂ O ₃	Fe ₂ O ₃	CaO	MgO	Na ₂ O	TiO ₂	K ₂ O	P ₂ O ₅	MnO
B16Ca _(glass)	36.11 (0.34)	12.19 (0.17)	10.06 (0.29)	24.44 (0.33)	9.19 (0.56)	2.28 (0.10)	2.02 (0.08)	1.12 (0.07)	0.46 (0.10)	0.15 (0.03)

The Raman spectrum of the parent glass may be divided in 3 parts (Figure 1). The low frequency range includes the boson peak between 50 and 150 cm⁻¹, linked to the rotation of silicate tetrahedra [37]. The high intensity region of the spectrum contains three broad bands: the low frequency envelope (LF), between 250 and 630 cm⁻¹, the middle frequency envelope (MF) between 630 and 785 cm⁻¹ and the high frequency envelope (HF) between 735 and 1250 cm⁻¹ (Figure 1). The LF envelope is related to vibrations of bridging oxygen in rings of tetrahedra (McMillan and Piriou, 1982; Mysen et al., 1980; Neuville, 2006; Neuville et al., 2014; Neuville and Mysen, 1996;

Pasquarello et al., 1998; Seifert et al., 1982; Umari et al., 2003). The MF corresponds to the intertetrahedral bending mode of polymerized species [45,46]. The HF envelope is attributed to the vibrations of T-O- bonds – where T stands for the fourfold coordinated cations Si^{4+} , Al^{3+} , Fe^{3+} or P^{5+} , and O⁻ for the non-bridging oxygen (NBO) – and the structural effect of network-modifying and charge-balancing cations [see references in [39], and [30,41,46–50]. All the vibrations of the HF region are convoluted in a single wide envelope. The ratio between the area of the HF and the LF envelopes shows that the glass is essentially depolymerized.

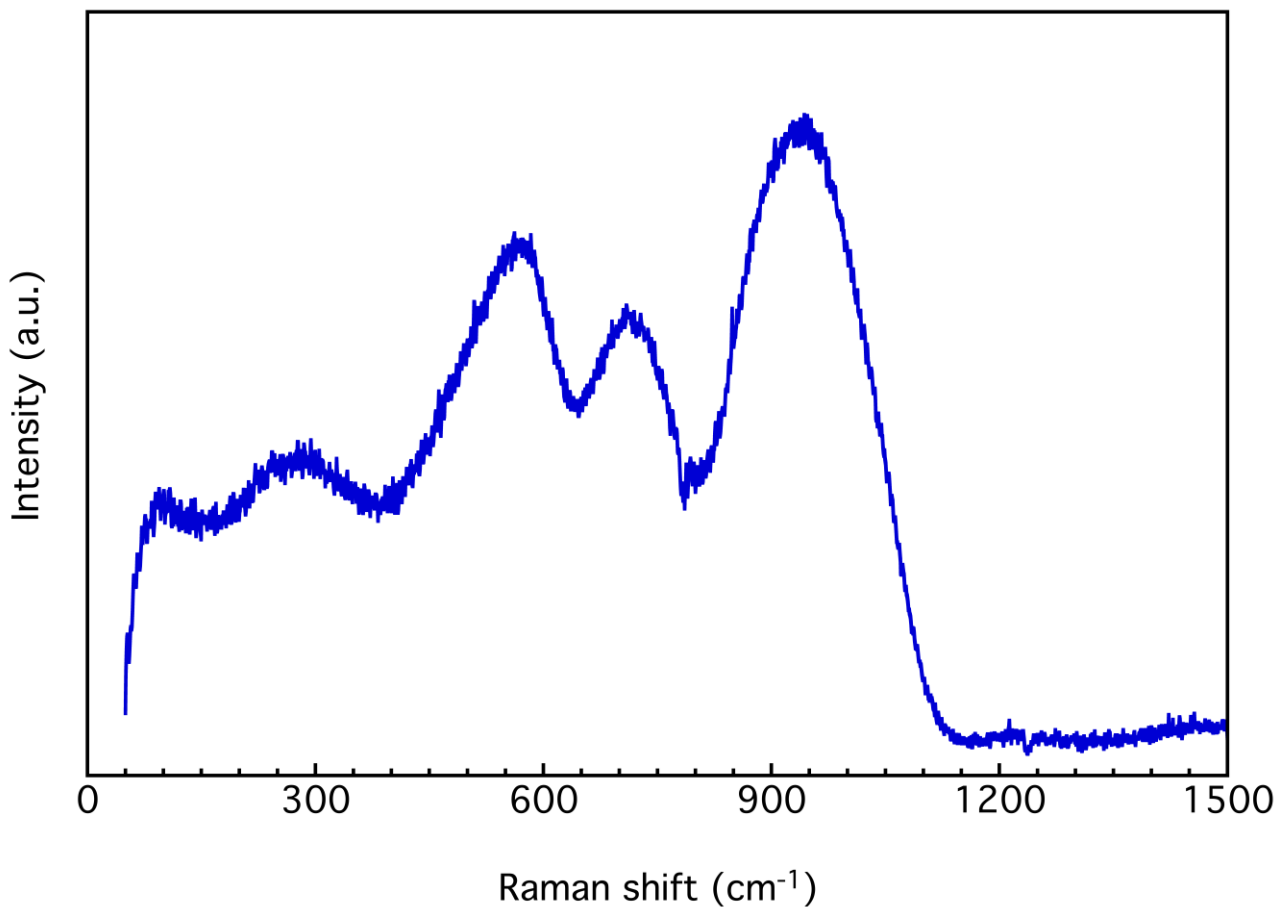


Figure 1. Unpolarized normalized Raman spectrum of the parent glass.

The thermal behavior of the original glass shows two exothermic events attributed to the formation of different mineral phases (Figure 2). The first signal is a sharp peak at 874 °C and the second is smaller, wider and located at 924 °C. An endothermic event at 1128 °C is linked to the melting of

the system (melting of akermanite). Glass transition temperature measured at 10 °C/min of the parent glass is 651 °C and its thermal expansion coefficient is $9.7 \cdot 10^{-6} \text{ } ^\circ\text{C}^{-1}$.

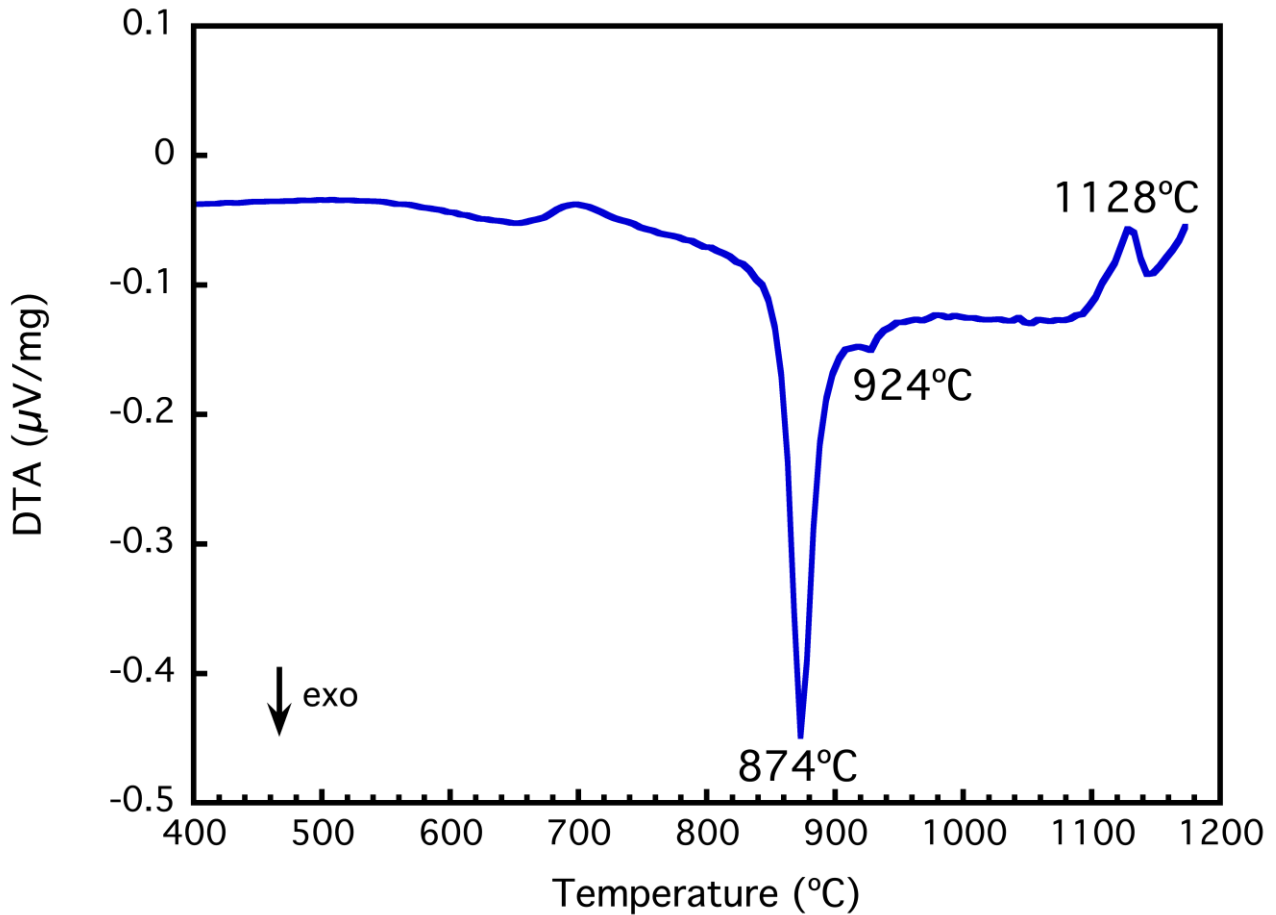


Figure 2. DTA plot of the original glass obtained using a heating rate of 10 °C/min.

3.2. Determination of the temperatures of maximum nucleation rate and crystal growth

The temperature of maximum nucleation rate can be obtained from the shift of the exothermic peak corresponding to crystallization when the glass is treated at different nucleation temperatures (T_N) [27]. This approach should supply T_N for each of the mineral phases that crystallize from the original glass. Two different events have been isolated. The first is a broad peak centered at 650 °C from the shift of the exothermic peak at 874 °C (Figure 3), which appears in all the analyses. The second is a narrower peak centered at 675 °C, which is only detected for T_N below 750 °C, corresponding to the variation of the peak at 924 °C (Figure 3).

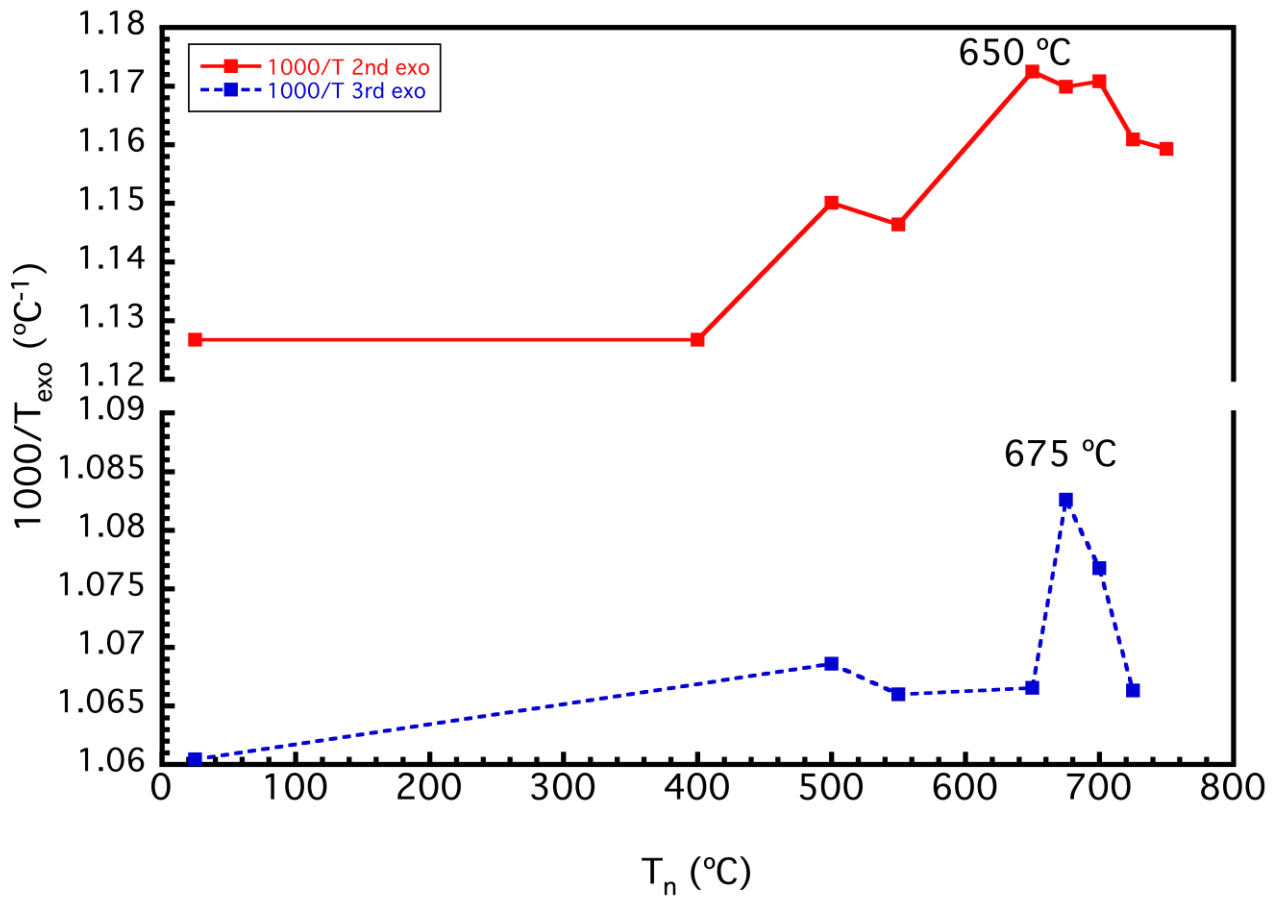


Figure 3. Plots representing the shift of the inverse of the temperature of the exothermic peak as a function of temperature corresponding to the two exothermic events.

The sequence of nucleation of the newly-formed minerals and the attribution of the T_{MNR} are studied from the evolution of the intensity of the main diffraction peak after a sudden heating at T_N and further heating up to the temperature of the exothermic event (T_{exo}) from DTA to induce crystal growth (Table 3 and Figure 4). The first T_{MNR} is attributed to the nucleation of magnetite (Fe_3O_4), as it has the most intense XRD peaks at 650 °C; its peak height later diminishes and becomes undetectable at 700 °C. Nepheline ($NaAlSiO_4$) starts nucleating at 650 °C and its nucleation rate is larger at 700 °C, but cannot be proved to be at its maximum at this temperature (Figure 4). The nucleation of diopside ($CaMgSi_2O_6$) and merwinite ($Ca_3MgSi_2O_8$) is fast and at about the same temperature range: between 650 °C and 700 °C. The proximity between all these nucleation events makes it difficult to attribute the T_{MNR} linked to the second event at 675 °C to a single phase with the available data, as they are probably overlapped (Figure 4).

Table 3. Intensities of the main diffraction peaks of the newly-formed mineral phases after sudden thermal treatments at the T_N followed by growth at the temperature of the first exothermic. The numbers below the mineral phases correspond to the Powder Diffraction File (PDF) used in the Rietveld refinement.

T_N (°C)	Newly-formed minerals (cps)				
	Magnetite	Nepheline	Diopside	Merwinite	Akermanite
	01-088-0315	01-076-2467	01-072-1379	01-089-2432	01-079-2424
600	113	-	-	-	-
650	301	63	431	-	-
700	165	167	265	-	-
750	-	1726	6001	2697	33
800	-	1450	5892	2218	1893

The intensities and narrowness of the XRD peaks at 750 and 800 °C, coupled with the apparent scarcity of residual glass, show that the nucleation stage has finished and crystal growth is the current /ongoing process. A new mineral phase, akermanite ($\text{Ca}_2\text{Mg}[\text{Si}_2\text{O}_7]$), is detected at 750 °C.

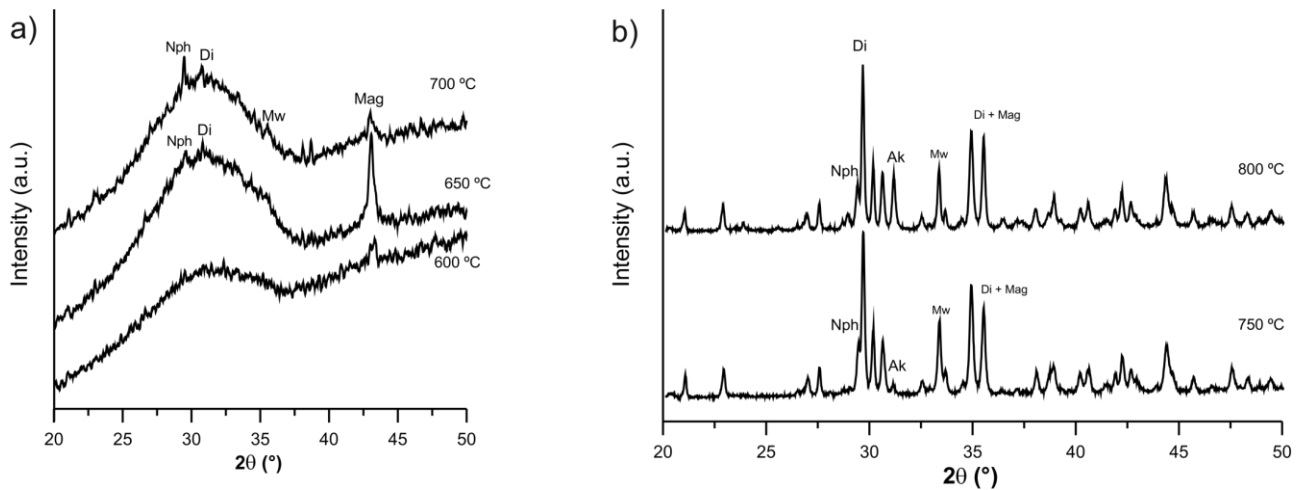


Figure 4. Sequence of XRD patterns obtained after a sudden heating of glass samples at a) T_{MNR} and b) T_{GR} for each phase. The temperatures in the plot correspond to the T_N of each treatment.

3.3. Evolution of the crystalline phases in the devitrification process

XRD spectra show the evolution of the newly-formed mineral phases between 770–1200 °C during devitrification of the original glass in in-situ HT-XRD. The sample stays amorphous up to 760 °C and the first diffraction peaks can be detected at 770 °C. The nucleation process is not controlled in

this experiment, hence the series of XRD patterns show both nucleation and growth of the minerals with increasing temperature (Figure 5).

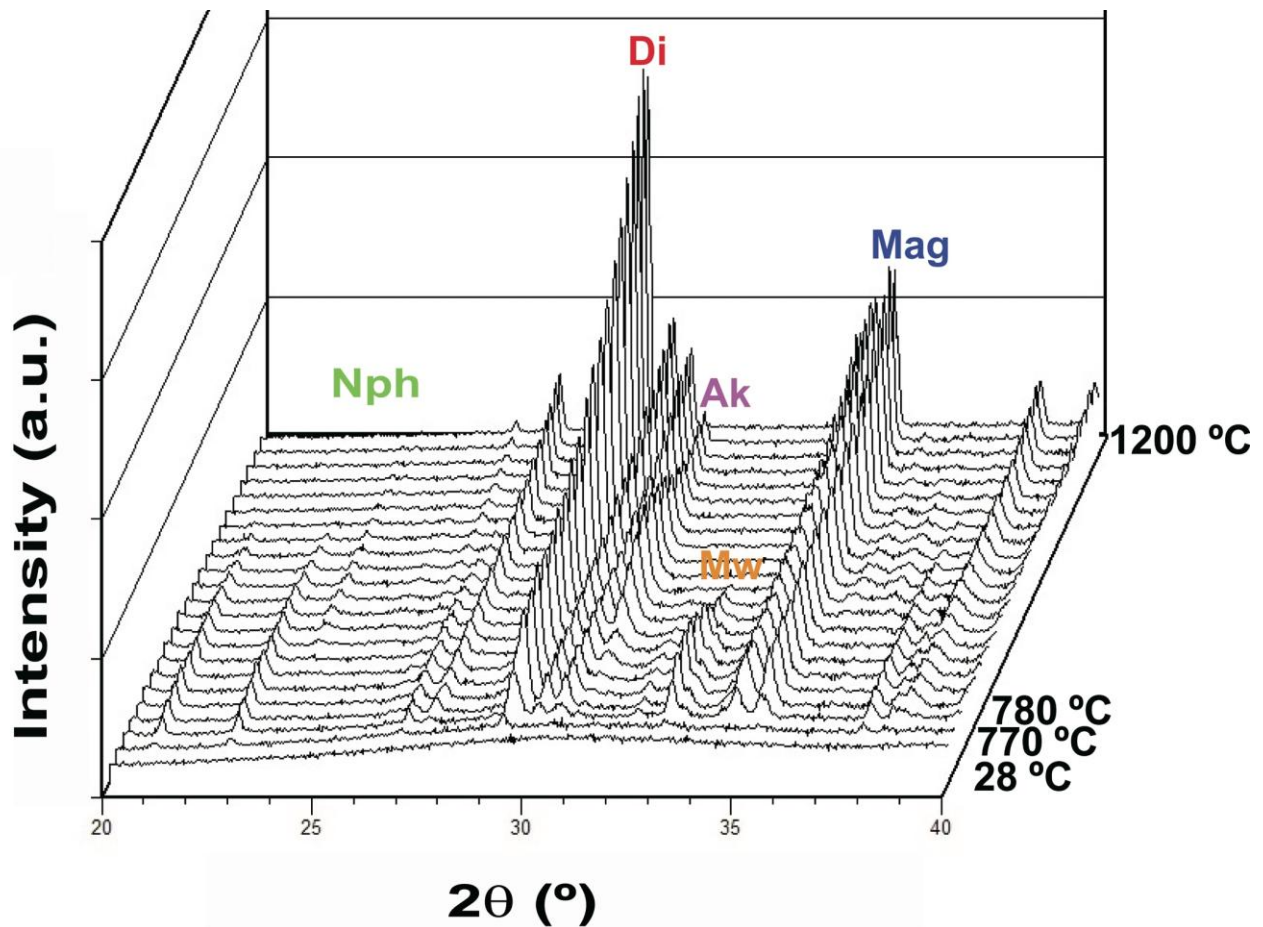


Figure 5. HT-XRD spectra in the range 2θ between 20 and 40 °.

Diopside, nepheline and merwinite can be seen in the HT-XRD spectrum at 770 °C, whereas akermanite is detected from 800 °C (Figure 5). The evolution of the intensity of each of the mineral phases has been tracked using the following diffraction peaks: d_{201} for nepheline, d_{310} for merwinite, d_{310} for diopside and d_{211} for akermanite (Figure 6). They are the most intense that did not overlap with peaks from coexistent phases. The evolution of magnetite could not be tracked in this experiment because its main diffraction peak overlaps with a major peak of diopside and the rest of reflections are not intense enough.

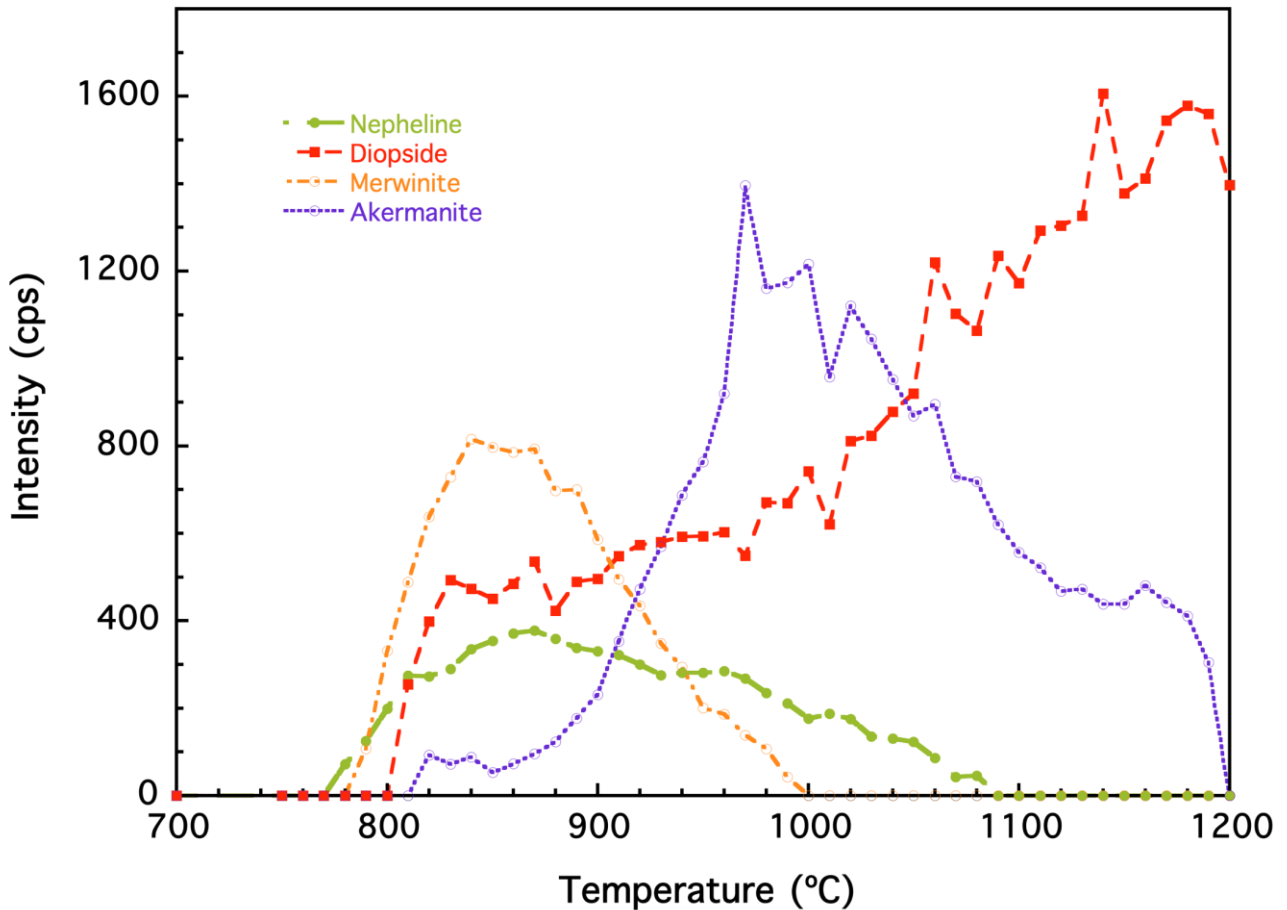


Figure 6. Evolution of the intensities of selected XRD peaks (d_{201} for nepheline, d_{310} for merwinite, d_{310} for diopside and d_{211} for akermanite) as a function of temperature.

Nepheline is stable between 760 °C and 1080 °C, with a maximum intensity at 860 °C. Merwinite has a similar behavior: it also reaches a maximum at 860 °C and becomes undetectable over 980 °C. The peak intensities of akermanite increases during the decrease of these two phases, reaches its maximum at 970 °C and becomes undetectable at 1190 °C. The peak intensity of diopside increases along the whole temperature range, alongside with the crystallization and melting reactions of merwinite and akermanite (Figure 5 and Figure 6). The sample does not undergo additional changes during cooling.

The sizes of coherent crystals at each temperature can be calculated using Scherrer's equation to establish the growth of each phase. The maximum crystal size reached in HT-XRD for all the minerals is between 40 – 70 nm. This can be due to the fact that all phases nucleate in a narrow

1 temperature range, hence forming a large number of nuclei before reaching the crystal growth
2 temperature (T_{GR}) and constraining crystal growth. Magnetite crystals are still smaller, reaching a
3 maximum of 18 nm. Its role is to act as a nucleus for the growth of diopside and it is absorbed
4 inside its structure to approach the Fe-rich end-member.
5
6
7
8
9

10 3.4. Evolution of the viscosity of the original glass as a function of nucleation time

11 The viscosity-temperature curves of samples treated at a nucleation temperature of 650 °C during
12 different periods of time (between 0 and 8 h) are traced using the fixed viscosity points from HSM
13 [34] (Figure 7). In general, a longer nucleation time increases the viscosity (for a nucleation period
14 between 0 and 4h), in the high viscosity range (between $10^{7.9-6.9}$ Pa·s). However, the sample treated
15 during 8 h is very similar to the sample nucleated for 2 h as the system becomes multiphasic with
16 the separation between two solid phases, one crystalline and one amorphous. However, increasing
17 nucleation time reduces the viscosity in the low viscosity range (between $10^{5.6-2.1}$ Pa·s). At 650 °C
18 the phases that will nucleate are magnetite and nepheline. The nucleation of nepheline will extract
19 Na and K from the glass, thus increasing the viscosity according to longer nucleation times. The
20 variation of viscosity is also conditioned by the effect of nucleation on the sintering process.
21 Between the first shrinkage ($10^{7.9}$ Pa·s) and the softening points ($10^{5.6}$ Pa·s), all matter will be in the
22 solid state, either as a crystalline or an amorphous phase. The shrinkage of the probe at this stage is
23 controlled by an evaporation-condensation process depending on vapor pressure. Increasing the
24 amount of nuclei will reduce vapor pressure because crystals have lower vapor pressure than
25 amorphous materials. The formation of nuclei requires increasing the vapor pressure by means of a
26 temperature rise for the sintering process to occur, which is in good agreement with the temperature
27 at which each sample reaches the maximum shrinkage point ($10^{6.9}$ Pa·s) increasing with nucleation
28 time.
29
30
31
32
33
34
35
36
37
38
39
40
41
42
43
44
45
46
47
48
49
50
51
52
53
54
55
56

57 For viscosities below the softening point, matter will be a mixture of solid crystals and a melt. In
58 these conditions, the main agent controlling viscosity is capillarity, defined as the interstitial energy
59
60
61
62
63
64
65

between solid and liquid [51]. In addition, a larger number of nepheline crystals will cause a more sudden decrease in viscosity upon its melting between 897 and 1080 °C. In the viscosity-temperature curves this corresponds to a drop between first shrinkage and softening, which can be correlated to the decrease in the viscosity of the melt caused by the incorporation of Na and K that have left the nepheline structure. The second, more gradual, viscosity drop is attached to a decrease in the crystal/liquid ratio, which is independent of nucleation time, as the curves are approximately parallel in this range (Figure 7).

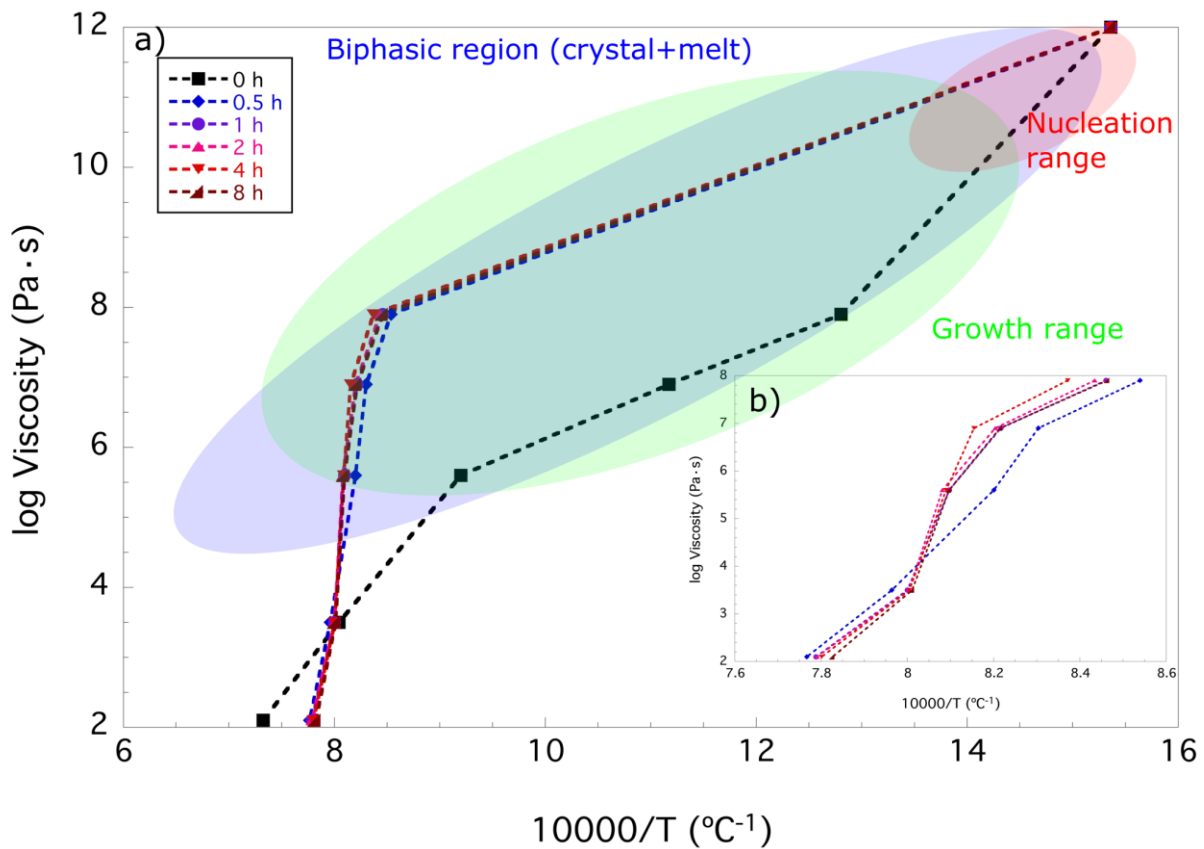


Figure 7. Viscosity-temperature curves for glasses with a) different nucleation times b) magnification focusing on the samples nucleated before the HSM experiments. The highlighted areas represent the biphasic region, where a crystal and a glass/melted phase coexist (purple), the nucleation range, which are XRD-amorphous (red) and the growth range, where crystallization increases viscosity as a function of the nucleation time (green).

3.5. Glass-ceramic characterization

The glass-ceramic has been obtained through the thermal treatment of the parent glass based on the T_N and T_{GR} exposed earlier. It is formed by nepheline (12.15 wt%), magnetite (6.03 wt%), diopside (41.32 wt%) and akermanite (40.50 wt%) (Figure 8).

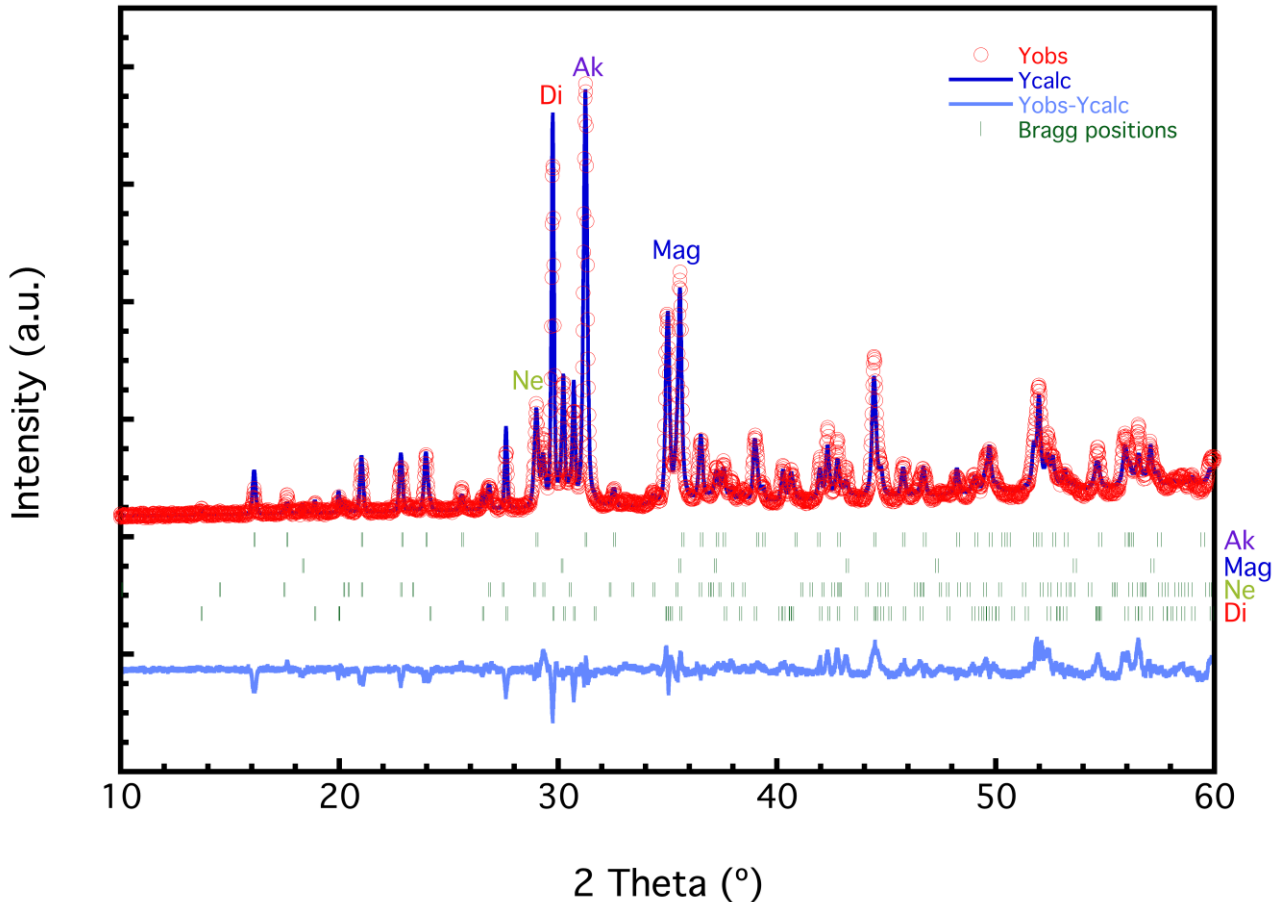


Figure 8. XRD pattern of the glass-ceramic showing the observed intensity (Yobs) of the experiment, the calculated intensity of the Rietveld refinement (Ycalc), the difference curve and the Bragg positions of the diffraction for each mineral phase. The labels identify the 100 % intensity diffraction peak of each crystalline phase.

Treating the parent glass at the T_{MNR} generates a large number of nuclei, which grow upon further heating. Between each T_N the heating is fast to minimize the growth of the phases that were nucleated in previous steps, ensuring a homogeneous crystal size. The bulk microstructure of the glass-ceramic observed on SEM consists on idiomorphic crystals ranging between 60 and 120 nm (Figure 9). Diopside, akermanite and nepheline form a homogeneous grain microstructure. Akermanite and diopside crystals have been distinguished by their Si/Ca ratio (higher in diopside

than in akermanite). The observed sizes of the crystals are larger than 40–70 nm obtained from Scherrer's equation for diopside, nepheline and akermanite and 18 nm for magnetite. This difference arises from the steps for crystallization during glass-ceramic production being much longer than for in-situ HT-XRD.

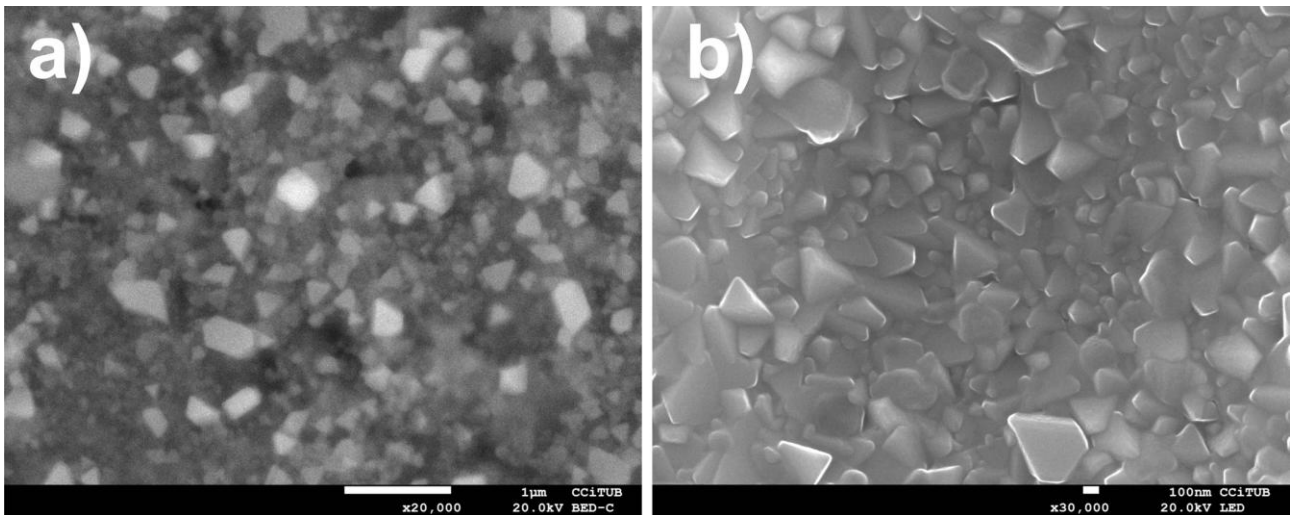


Figure 9. SEM micrographs showing the texture of the glass-ceramic. a) a BDS image of the mass of the crystals where dense magnetite crystals stand out b) a detail of the mixture of fine grained idiomorphic diopside, akermanite and nepheline.

3.6. Microhardness

The Vickers microindentation test has given a microhardness of 8.2 GPa for the parent glass and of 8.6 GPa for the glass-ceramic. These values lie in the hardness range of the diopside-hedenbergite series (from 7.7 to 9.8 GPa), are higher than the augite series (from 6.6 to 8.0), and considerably higher than the hardness of akermanite (5.2 to 6.6 GPa). The abundance of diopside is the main contributor to the increase of the microhardness, which leads to an improvement on the mechanical properties of the obtained material.

3.7. Leaching

The glass-ceramic process has increased the overall stability of the glass, as the concentration of most of the elements in the glass-ceramic leachate are lower than in the glass leachate (Table 4). However, the leachability of elements such as Ca, Si, Zn and Pb, As and Cd is higher from the glass-ceramic than the glass. The concentration of each element in the leachates is several orders of magnitude below their concentrations in the original basalts.

Table 4. Concentration of selected elements on the leachates after blank subtraction. BB stands for “below blank concentration” and BDL for “below detection limit”.

[ppm] in solution	Ca	K	Si	Na	Mg	Fe	Al	Ba	P
Glass	3.52	2.24	4.17	9.73	2.73	0.39	1.18	0.04	BB
Glass-ceramic	4.43	1.88	4.79	8.31	2.45	0.11	0.88	0.09	BB

[ppb] in solution	Zn	Pb	As	Cu	Cr	Ni	Cd	Ti
Glass	BB	0.83	0.23	11.09	BDL	9.00	BB	76.32
Glass-ceramic	2.85	1.04	0.71	10.68	BDL	7.16	0.18	26.73
DIN 38414-S4 [30]	4000	500	500	2000	500	400	40	N/A

4. Discussion

The composition of the parent glass corresponds to the border between the stability fields of pyroxene and melilite in the section at 10 wt% Al_2O_3 of the phase diagram of the system $\text{CaO-Al}_2\text{O}_3\text{-MgO-SiO}_2$, the major glass components. The crystallization of akermanite – the magnesian end-member of the melilite solid solution $((\text{Ca,Na})(\text{Al,Mg,Fe}^{2+})[(\text{Al,Si})\text{SiO}_7])$ – and its relationship with merwinite is a controversial question in the literature [22] consider merwinite a metastable phase formed during the thermal treatments of multicomponent glasses in the initial stages of the devitrification process, around T_g . The relaxation of the glass structure upon at higher temperatures will facilitate the diffusion of ions [14] causing the destabilization of merwinite, which will react with the other minerals to produce the stable mineral phases according to the phase diagram of the system [52].

1 A study of the crystallization of a glass of a composition in the akermanite-gehlenite system
2 (2CaO·(1-x)·MgO·xAl₂O₃·(2-x)SiO₂) proved that merwinite is a metastable phase for all x below or
3 equal to 0.6 and attributed this fact to structural reasons [53]. In the case of the melilite minerals,
4 corresponding to the sorosilicate group, the structure consists in a fragmented network of silica
5 tetrahedra and modifier cations are stabilized by the ionic bonds between the tetrahedra and the
6 cations [22]. Merwinite is a nesosilicate and thus presents a lower concentration of silica tetrahedra,
7
8 creating a less strong network that melts at lower temperature [53]. The formation of akermanite
9
10 may then be explained from the diffusion of calcium from merwinite to diopside described by the
11
12 following reaction:
13
14
15
16
17
18
19

20 Merwinite + Diopside → Akermanite
21



26 The bulk composition of the parent glass can be expressed as 2CaO·1.05MgO·0.55Al₂O₃·2.76SiO₂
27 using the formula of melilite. In this case, x is effectively below 0.6 and then merwinite is
28 metastable. Moreover, the already insufficient concentration of Al in the system is also influenced
29 by the formation of nepheline during the devitrification process. Nepheline is the phase with a
30 higher Al concentration between those formed during the devitrification process hence its formation
31 extracts Al from the system, destabilizing merwinite and enhancing the crystallization of
32 akermanite. Even the melting of nepheline over 860 °C does not introduce enough Al in the system
33 to allow the formation of merwinite, and thus it is absent from the glass-ceramic.
34
35
36
37
38
39
40
41
42
43
44

45 Nucleation and crystallization influence macroscopic properties of the melt such as viscosity [54],
46 which are essential in the production of the glass and the glass-ceramic. The large increase in
47 viscosity between the parent and the nucleated glasses is attributed to the formation of a biphasic
48 system consisting in a crystalline and an amorphous phase. The crystals facilitate the formation of
49 the fine-grained glass-ceramic by hampering the viscous flow at the nucleation range, limiting the
50 reactivity between the different phases (Figure 7) in a similar manner. A further temperature rise
51 decreases the bulk viscosity of the material permitting reactions between minerals but preserving
52
53
54
55
56
57
58
59
60
61
62
63
64
65

the fine microstructure until the melting range (around 10^3 Pa·s), where the system becomes monophasic again. Villeneuve and coworkers observed a similar behavior in their viscosity measurements during nucleation processes on basaltic melts of Piton de la Fournaise volcano [55].

The production process of the glass-ceramic based on the determination of the temperatures of maximum nucleation rates and the study of crystal growth has provided a crystalline material with a fine microstructure. Obtaining extensive nucleation on a glass-ceramic based on basalt usually requires a $\text{Fe}_2\text{O}_3/\text{FeO}$ ratio over 0.5 [56]. The raw basalt $\text{Fe}_2\text{O}_3/\text{FeO}$ equals 0.501 [57] and supplementary oxidation is provided by melting the ground basalt under air atmosphere [18]. This fine microstructure is a direct result of the treatment of the glass at the temperatures of maximum nucleation rate for an extended period (in this case, 6 h) followed by a fast heating of the sample up to the growth temperature to avoid the formation of metastable phases such as merwinite. An additional factor that may help in developing this microstructure is the presence of pre-structured domains as hinted by the noisy Raman signal. The presence of magnetite and diopside in the mineralogy of the glass-ceramic shows a good potential for the inertization of PTE such as Cr or Zn present in sludge [10–12] because they could be hosted in the spinel structure or in the pyroxene lattice.

The microhardness of the glass and the glass-ceramic lie on the same range, and near the higher limit, of the reported values for basalt glasses and glass-ceramics in the literature (Table 5). The extensive nucleation of the parent glass creates a fine microstructure and limits the eventual formation of porosity due to crystal growth, making the glass-ceramic harder than the glass in spite of bearing approximately 40 wt% of the soft mineral akermanite (5.2–6.6 GPa). These results have to be taken with certain reserve because the difference in hardness between B16Ca glass and glass-ceramic is within the experimental error. However, the trend of increasing hardness is a promising advocate for the glass-ceramic process as a means for improving the mechanical properties of multicomponent glass.

Table 5. Microhardness results of this study compared to Vickers microhardness values for basaltic glasses and glass-ceramics in a [58], b [59], and c [60].

Material	Vickers Microhardness (GPa)
Sant Joan les Fonts Basalt glass	7.7 ± 0.3
B16Ca glass	8.2 ± 0.5
B16Ca glass-ceramic	8.6 ± 0.5
Canary Island Basalt glass (a)	5.16 – 6.28
Canary Island Basalt glass-ceramic (a)	6.62 – 8.66
Basalt rock fiber glass (b)	7.7
Basalt glass/crystal mixtures (b)	6.8 – 8.9
Holyoke basalt glass (c)	8.9

Glass-ceramics are generally characterized by a good chemical resistance, comparable to other ceramic materials [61]. In this study, the leachability tests provided complex results. The decrease in the concentrations of most of the main components between the leachates of the glass and the glass-ceramic point to an overall better inertization potential. However, the leachability of Ca, Si, Zn, Pb, As and Cd is lower in the glass than in the glass-ceramic. Fredericci and coworkers observed a similar situation in the increase of weight loss between a blast furnace slag glass and glass-ceramics [22]. This situation might be caused by the high amount of akermanite, which is the phase with higher Ca and Si contents of the glass-ceramic. Karamanov and coworkers produced a diopside glass-ceramic which underwent a weight loss as low as 0.3 wt% [62], whereas 1.2 wt% losses have been reported for acid-resistant melilite glass-ceramics [22]. Therefore, a line emerging from this research could focus on decreasing the amount of Ca to increase the proportion of pyroxene and maximize the chemical resistance of the glass-ceramic.

5. Conclusions

We achieved the vitrification of a Ca-rich basalt analogous to sewage sludge and its transformation into a diopside-akermanite-magnetite-bearing glass-ceramic based on the determination of the temperatures of maximum nucleation rate and crystal growth of the newly-formed phases. The glass-ceramic process enhances the microhardness of the product, which lies in the upper part of the

1 literature values for ceramic tiles where abrasion-resistant materials are required such as the
2 building industry. Optimizing the leachability in the glass-ceramic may require adjusting the
3 concentration of calcium to reduce the crystallization of akermanite, promoting the formation of
4 more spinel-like phases and pyroxene. Concerning the production process, the apparent viscosity of
5 the system increases as it becomes biphasic during nucleation and crystallization. This confers a
6 certain rigidity to the material, limiting the reactions between formed nuclei and the residual liquid
7 phase until crystallization is finished. The result is a nanometric homogeneous microstructure
8 responsible for the enhanced mechanical properties of the glass-ceramic. Both the glass and the
9 glass-ceramic effectively bind the PTE in their structures in compliance with European legislation –
10 in the glass structure and the crystalline lattices of the spinel-group and pyroxene minerals
11 respectively. The designed process opens the way to use sewage sludge-like waste as raw materials
12 for environmentally safe products, with the additional advantage of reducing the need for their
13 mining.

32 **6. Acknowledgements**

33 This research was supported by Consolidated Group for Structure and Materials Desing ,
34 2017SGR1687 and by the Fundació Bosch i Gimpera Project 307466. The authors would like to
35 thank the staff of the Centres Científics i Tecnològics of the University of Barcelona (CCiTUB) for
36 their technical support and Esther Vilalta and the Departament de Ciència de Materials i Enginyeria
37 Metal·lúrgica for the access to the Vickers microindenter. M. Tarragó received support from a PhD
38 grant from the Ministerio de Educación, Cultura y Deporte (FPU13/04507).

52 **7. References**

- 53 [1] EPA, Land Application of Sewage Sludge, Fed. Regist. (1994).
54 [55 http://water.epa.gov.akadns.net/polwaste/wastewater/treatment/biosolids/upload/2002_06_28](http://water.epa.gov.akadns.net/polwaste/wastewater/treatment/biosolids/upload/2002_06_28)
56 [57 _mtb_biosolids_sludge.pdf](http://water.epa.gov/polwaste/wastewater/treatment/biosolids/_mtb_biosolids_sludge.pdf)
58 [59 http://water.epa.gov/polwaste/wastewater/treatment/biosolids](http://water.epa.gov/polwaste/wastewater/treatment/biosolids)

ds/upload/2002_06_28_mtb_biosolids_sludge.pdf.

- 1 [2] Agència Catalana de l'Aigua, Evolució de les dades de la producció i de la gestió dels fangs
2
3
4 ., (2015). <https://aca->
5
6 [web.gencat.cat/aca/documents/ca/actuacions/sistemes_sanejament/com_funcionen_edars/evo](https://aca-web.gencat.cat/aca/documents/ca/actuacions/sistemes_sanejament/com_funcionen_edars/evo)
7
8 [l_fangs_web.pdf](https://aca-web.gencat.cat/aca/documents/ca/actuacions/sistemes_sanejament/com_funcionen_edars/evo) (accessed February 6, 2017).
9
- 10 [3] V.J. Inglezakis, A.A. Zorpas, A. Karagiannidis, P. Samaras, I. Voukkali, S. Sklari,
11
12 EUROPEAN UNION LEGISLATION ON SEWAGE SLUDGE MANAGEMENT, 23
13
14 (2016) 635–639.
15
16
- 17 [4] M. Romero, J.M. Rincón, Microstructural characterization of a goethite waste from zinc
18
19 hydrometallurgical process, *Mater. Lett.* 31 (1997) 67–73. doi:10.1016/S0167-
20
21 577X(96)00235-2.
22
23
24
- 25 [5] M. Garcia-Valles, G. Avila, S. Martinez, R. Terradas, J.M. Nogues, Heavy metal-rich wastes
26
27 sequester in mineral phases through a glass-ceramic process, *Chemosphere.* 68 (2007) 1946–
28
29 1953. doi:10.1016/j.chemosphere.2007.02.034.
30
31
- 32 [6] M. Tarrago, M. Garcia-Valles, M.H.H. Aly, S. Martinez, Valorization of sludge from a
33
34 wastewater treatment plant by glass-ceramic production, *Ceram. Int.* 43 (2017) 930–937.
35
36 doi:10.1016/j.ceramint.2016.10.083.
37
38
- 39 [7] T.A. Guillemet, P. Maesen, E. Delcarte, G.C. Lognay, A. Gillet, J.J. Claustrioux, M. Culot,
40
41 Factors influencing microbiological and chemical composition of South-Belgian raw sludge,
42
43 *Biotechnol. Agron. Soc. Environ.* 13 (2009) 249–255.
44
45 <http://www.scopus.com/inward/record.url?eid=2-s2.0->
46
47 [70049084577&partnerID=40&md5=6d80b3f51734780da3affb02c32b2494](http://www.scopus.com/inward/record.url?eid=2-s2.0-70049084577&partnerID=40&md5=6d80b3f51734780da3affb02c32b2494).
48
49
50
51
- 52 [8] M.I. Ansari, A. Malik, Seasonal variation of different microorganisms with nickel and
53
54 cadmium in the industrial wastewater and agricultural soils, *Environ. Monit. Assess.* 167
55
56 (2010) 151–163. doi:10.1007/s10661-009-1038-y.
57
58
- 59 [9] N. Hecht, D. Duvall, Characterization and Utilization of municipal and utility sludges and
60
61
62
63
64
65

ashes, 1975.

- 1 [10] M.K. Hossain, V. Strezov, P.F. Nelson, Thermal characterisation of the products of
2 wastewater sludge pyrolysis, *J. Anal. Appl. Pyrolysis*. 85 (2009) 442–446.
3
4 doi:10.1016/j.jaap.2008.09.010.
5
6
7
8 [11] T. Tervahauta, S. Rani, L. Hernández Leal, C.J.N. Buisman, G. Zeeman, Black water sludge
9 reuse in agriculture: Are heavy metals a problem?, *J. Hazard. Mater.* 274 (2014) 229–236.
10
11 doi:10.1016/j.jhazmat.2014.04.018.
12
13
14 [12] R.D. Rawlings, J.P. Wu, A.R. Boccaccini, Glass-ceramics: Their production from wastes-A
15 Review, *J. Mater. Sci.* 41 (2006) 733–761. doi:10.1007/s10853-006-6554-3.
16
17
18 [13] S. Suzuki, M. Tanaka, T. Kaneko, Glass-ceramic from sewage sludge ash, *J. Mater. Sci.* 2
19 (1997) 1775–1779. doi:10.1023/a:1018584202392.
20
21
22 [14] M. Erol, S. Küçükbayrak, A. Ersoy-Meriçboyu, Production of glass-ceramics obtained from
23 industrial wastes by means of controlled nucleation and crystallization, *Chem. Eng. J.* 132
24 (2007) 335–343. doi:10.1016/j.cej.2007.01.029.
25
26
27 [15] S. Do Yoon, Y.H. Yun, Preparation of glass ceramics from sludge bottom ash and waste
28 glass, *J. Ceram. Process. Res.* 12 (2011) 361–364.
29
30
31 [16] J.M. Juoi, D. Arudra, Z.M. Rosli, K. Hussain, A. Japper Jaafar, Microstructural properties of
32 glass composite material made from incinerated scheduled waste slag and soda lime silicate
33 (SLS) waste glass, *J. Non. Cryst. Solids*. 367 (2013) 8–13.
34
35
36 doi:10.1016/j.jnoncrysol.2013.02.004.
37
38 [17] M. Tarrago, M. Garcia-Valles, S. Martínez, D.R. Neuville, Phosphorus solubility in basaltic
39 glass: Limitations for phosphorus immobilization in glass and glass-ceramics, *J. Environ.*
40
41
42
43
44
45
46
47
48
49
50
51
52
53
54
55
56
57
58
59
60
61
62
63
64
65

and phase separation: from research to applications, 2017.

- 1 [20] N. Pavluskin, Vitrokeramik. Grundlagen der Technologie, 1986.
- 2
- 3 [21] G. Agarwal, R.F. Speyer, Devitrification hardening of cupola slag glass with CaO and SiO₂
- 4
- 5 additions, J. Non. Cryst. Solids. 135 (1991) 95–104. doi:10.1016/0022-3093(91)90409-Y.
- 6
- 7
- 8 [22] C. Fredericci, E.D. Zanutto, E.C. Ziemath, Crystallization mechanism and properties of a
- 9
- 10 blast furnace slag glass, J. Non. Cryst. Solids. 273 (2000) 64–75. doi:10.1016/S0022-
- 11
- 12 3093(00)00145-9.
- 13
- 14
- 15 [23] J.R.H. Arancibia, P. Alfonso, M. García-Valles, S. Martínez, D. Parcerisa, C. Canet, F.M.
- 16
- 17 Romero, Obtención de vidrio a partir de residuos de la minería del estaño en Bolivia, Bol. La
- 18
- 19 Soc. Esp. Ceram. y Vidr. 52 (2013) 143–150. doi:10.3989/cyv.192013.
- 20
- 21
- 22 [24] J. Shi, H. Feng, C. Ye, L. Hu, J. Xie, H. Yang, X. Liu, Preparation and characterization of
- 23
- 24 CaO·Al₂O₃·SiO₂ glass-ceramics from molybdenum tailings, Mater. Chem. Phys. 197 (2017)
- 25
- 26 57–64. doi:http://dx.doi.org/10.1016/j.matchemphys.2017.05.028.
- 27
- 28
- 29 [25] P. Alfonso, D. Castro, M. Garcia-Valles, M. Tarrago, O. Tomasa, S. Martinez, Recycling of
- 30
- 31 tailings from the Barruecopardo tungsten deposit for the production of glass, J. Therm. Anal.
- 32
- 33 Calorim. (2016). doi:10.1007/s10973-016-5332-y.
- 34
- 35
- 36 [26] P. Alfonso, O. Tomasa, M. Garcia-Valles, M. Tarrago, S. Martínez, H. Esteves, Potential of
- 37
- 38 tungsten tailings as glass raw materials, Mater. Lett. 228 (2018).
- 39
- 40
- 41
- 42
- 43
- 44
- 45 [27] X.J. Xu, C.S. Ray, D.E. Day, Nucleation and crystallization of Na₂O-2CaO-3SiO₂ glass by
- 46
- 47 differential thermal analysis, J. Am. Ceram. Soc. 74 (1991) 909–914. doi:10.1111/j.1151-
- 48
- 49 2916.1991.tb04321.x.
- 50
- 51
- 52 [28] D.A. Long, Raman spectroscopy, McGraw-Hill, 1977.
- 53
- 54
- 55 [29] C. Le Losq, D.R. Neuville, R. Moretti, J. Roux, Determination of water content in silicate
- 56
- 57 glasses using Raman spectrometry: Implications for the study of explosive volcanism, Am.
- 58
- 59 Mineral. 97 (2012) 779–790. doi:10.2138/am.2012.3831.
- 60
- 61
- 62
- 63
- 64
- 65

- 1
2
3
4
5
6
7
8
9
10
11
12
13
14
15
16
17
18
19
20
21
22
23
24
25
26
27
28
29
30
31
32
33
34
35
36
37
38
39
40
41
42
43
44
45
46
47
48
49
50
51
52
53
54
55
56
57
58
59
60
61
62
63
64
65
- [30] C. Le Losq, D.R. Neuville, P. Florian, G.S. Henderson, D. Massiot, The role of Al³⁺ on rheology and structural changes in sodium silicate and aluminosilicate glasses and melts, *Geochim. Cosmochim. Acta.* 126 (2014) 495–517. doi:10.1016/j.gca.2013.11.010.
- [31] A. Monshi, M.R. Foroughi, M.R. Monshi, Modified Scherrer Equation to Estimate More Accurately Nano-Crystallite Size Using XRD, *World J. Nano Sci. Eng.* 02 (2012) 154–160. doi:10.4236/wjnse.2012.23020.
- [32] J. Rodríguez-Carvajal, Recent advances in magnetic structure determination by neutron powder diffraction, *Phys. B Condens. Matter.* 192 (1993) 55–69. doi:10.1016/0921-4526(93)90108-I.
- [33] M. Garcia-Valles, H.S. Hafez, I. Cruz-Matias, E. Verges, M.H. Aly, J. Nogues, D. Ayala, S. Martinez, Calculation of viscosity-temperature curves for glass obtained from four wastewater treatment plants in Egypt, *J. Therm. Anal. Calorim.* 111 (2013) 107–114. doi:10.1007/s10973-012-2232-7.
- [34] M.J. Pascual, L. Pascual, A. Duran, Determination of the viscosity-temperature curve for glasses on the basis of the fixed viscosity points determined by hot stage microscopy, *Phys. Chem. Glas.* 42 (2001) 61–66.
- [35] DIN-38414S4, Deutsche Einheitsverfahren zur Wasser, Abwasser und Schlammuntersuchung, Bestimmung der Eluierbarkeit von Wasser (S4), in: 1984.
- [36] M. Tarrago, H. Esteves, M. Garcia-Valles, S. Martínez, D.R. Neuville, Effect of Ca in P-doped basaltic glass-ceramics: Application to waste inertization, *Mater. Lett.* 220 (2018) 266–268. doi:10.1016/j.matlet.2018.03.020.
- [37] B. Hehlen, E. Courtens, A. Yamanaka, K. Inoue, Nature of the Boson peak of silica glasses from hyper-Raman scattering, *J. Non. Cryst. Solids.* 307–310 (2002) 87–91. doi:10.1016/S0022-3093(02)01444-8.
- [38] P.F. McMillan, B. Piriou, The structures and vibrational spectra of crystals and glasses in the silica-alumina system, *J. Non. Cryst. Solids.* 53 (1982) 279–298. doi:10.1016/0022-

3093(82)90086-2.

- 1 [39] D.R. Neuville, D. de Ligny, G.S. Henderson, Advances in Raman Spectroscopy Applied to
2 Earth and Material Sciences, *Rev. Mineral. Geochemistry*. 78 (2014) 509–541.
3
4
5
6 doi:10.2138/rmg.2013.78.13.
7
- 8 [40] F.A. Seifert, B.O. Mysen, D. Virgo, Three-dimensional network structure of quenched melts
9 (glass) in the systems $\text{SiO}_2\text{-NaAlO}_2$, $\text{SiO}_2\text{-CaAl}_2\text{O}_4$ and $\text{SiO}_2\text{-MgAl}_2\text{O}_4$, *Am. Mineral*. 67
10 (1982) 696–717.
11
12
13
14
- 15 [41] D.R. Neuville, B.O. Mysen, Role of aluminium in the silicate network: In situ, high-
16 temperature study of glasses and melts on the join $\text{SiO}_2\text{-NaAlO}_2$, *Geochim. Cosmochim.*
17 *Acta*. 60 (1996) 1727–1737. doi:10.1016/0016-7037(96)00049-X.
18
19
20
21
22
- 23 [42] B.O. Mysen, D. Virgo, C.M. Scarfe, Relations between anionic structure and viscosity of
24 silicate melts - A Raman spectroscopic study, *Am. Mineral*. 65 (1980) 690–710.
25
26
27
- 28 [43] A. Pasquarello, J. Sarnthein, R. Car, Dynamic structure factor of vitreous silica from first
29 principles: Comparison to neutron-inelastic-scattering experiments, *Phys. Rev. B - Condens.*
30 *Matter Mater. Phys.* 57 (1998) 14133–14140. doi:10.1103/PhysRevB.57.14133.
31
32
33
34
- 35 [44] P. Umari, X. Gonze, A. Pasquarello, Concentration of Small Ring Structures in Vitreous
36 Silica from a First-Principles Analysis of the Raman Spectrum, *Phys. Rev. Lett.* 90 (2003) 4.
37
38
39
40
41
42
43
44
45
46
47
48
49
50
51
52
53
54
55
56
57
58
59
60
61
62
63
64
65
- [47] C. Le Losq, D.R. Neuville, Effect of the Na/K mixing on the structure and the rheology of
tectosilicate silica-rich melts, *Chem. Geol.* 346 (2013) 57–71.
doi:10.1016/j.chemgeo.2012.09.009.

- 1
2
3
4
5
6
7
8
9
10
11
12
13
14
15
16
17
18
19
20
21
22
23
24
25
26
27
28
29
30
31
32
33
34
35
36
37
38
39
40
41
42
43
44
45
46
47
48
49
50
51
52
53
54
55
56
57
58
59
60
61
62
63
64
65
- [48] R.J. Bell, P. Dean, Localization of phonons in vitreous silica and related glasses, *Int. Conf. Phys. Non-Crystalline Solids.* 22 (1972) 375–382.
- [49] T. Furukawa, K.E. Fox, W.B. White, intensities and structural units in sodium silicate glasses Raman spectroscopic investigation of the structure of silicate glasses . III . Raman intensities and structural units in sodium silicate glasses 8), 3226 (2011). doi:10.1063/1.442472.
- [50] B.O. Mysen, M.J. Toplis, Structural behavior of Al³⁺ in peralkaline, metaluminous, and peraluminous silicate melts and glasses at ambient pressure, *Am. Mineral.* 92 (2007) 933–946. doi:10.2138/am.2007.2334.
- [51] W.D. Kingery, *Introduction to ceramics*, Wiley, 1960.
- [52] E.M. Levin, H.F. McMurdie, *Phase diagrams for ceramists 1975 Supplement*, The American Ceramic Society, 1975.
- [53] P. Orsini, A. Buri, A. Marotta, Devitrification of Glasses in the Akermanite-Gehlenite System, *J. Am. Ceram. Soc.* 58 (1974) 306–311.
- [54] K.D. Kim, S.H. Lee, H.K. Ahn, Observation of nucleation effect on crystallization in lithium aluminosilicate glass by viscosity measurement, *J. Non. Cryst. Solids.* 336 (2004) 195–201. doi:10.1016/j.jnoncrysol.2004.01.001.
- [55] N. Villeneuve, D.R. Neuville, P. Boivin, P. Bachèlery, P. Richet, Magma crystallization and viscosity: A study of molten basalts from the Piton de la Fournaise volcano (La Réunion island), *Chem. Geol.* 256 (2008) 241–250. doi:10.1016/j.chemgeo.2008.06.039.
- [56] G.H. Beall, H.L. Rittler, BASALT GLASS CERAMICS., *Am. Ceram. Soc. Bull.* 55 (1976) 579–582.
- [57] P. Alfonso, *Mineralogía y aptitudes vitrocerámicas de materiales magmáticos neógenos de Cataluña*, 1985.
- [58] I. De Vicente Mingarro, *Estudio de los mecanismos de nucleación y cristalización en vidrios obtenidos a partir de rocas basálticas canarias*, 1992.
- [59] M. Jensen, M.M. Smedskjaer, M. Estrup, M. Kristjansson, N. Lönnroth, Y.Z. Yue, *Hardness*

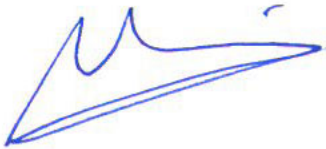
of basaltic glass-ceramics, *Glas. Technol. Eur. J. Glas. Sci. Technol. Part A.* 50 (2009) 189–195.

- 1
2
3
4 [60] A.W.A. El-Shennawi, M.A. Mandour, M.M. Morsi, S.A.M. Abdel-Hameed, Monopyroxenic
5
6 basalt-based glass-ceramics, *J. Am. Ceram. Soc.* 82 (1999) 1181–1186. doi:10.1111/j.1151-
7
8 2916.1999.tb01893.x.
9
- 10 [61] P.F. McMillan, B. Piriou, *Glass Ceramics*, Academic Press, 1975.
11
- 12 [62] A. Karamanov, I. Gutzow, I. Penkov, J. Andreev, B. Bogdanov, Diopside marble-like
13
14 sintered glass- ceramics, *Glas. Berichte Glas. Sci. Technol.* 67 (1994) 202–206.
15
16
17
18
19
20
21
22
23
24
25
26
27
28
29
30
31
32
33
34
35
36
37
38
39
40
41
42
43
44
45
46
47
48
49
50
51
52
53
54
55
56
57
58
59
60
61
62
63
64
65

Declaration of interests

The authors declare that they have no known competing financial interests or personal relationships that could have appeared to influence the work reported in this paper.

The authors declare the following financial interests/personal relationships which may be considered as potential competing interests:



Mariona Tarrago

Figure 1
[Click here to download high resolution image](#)

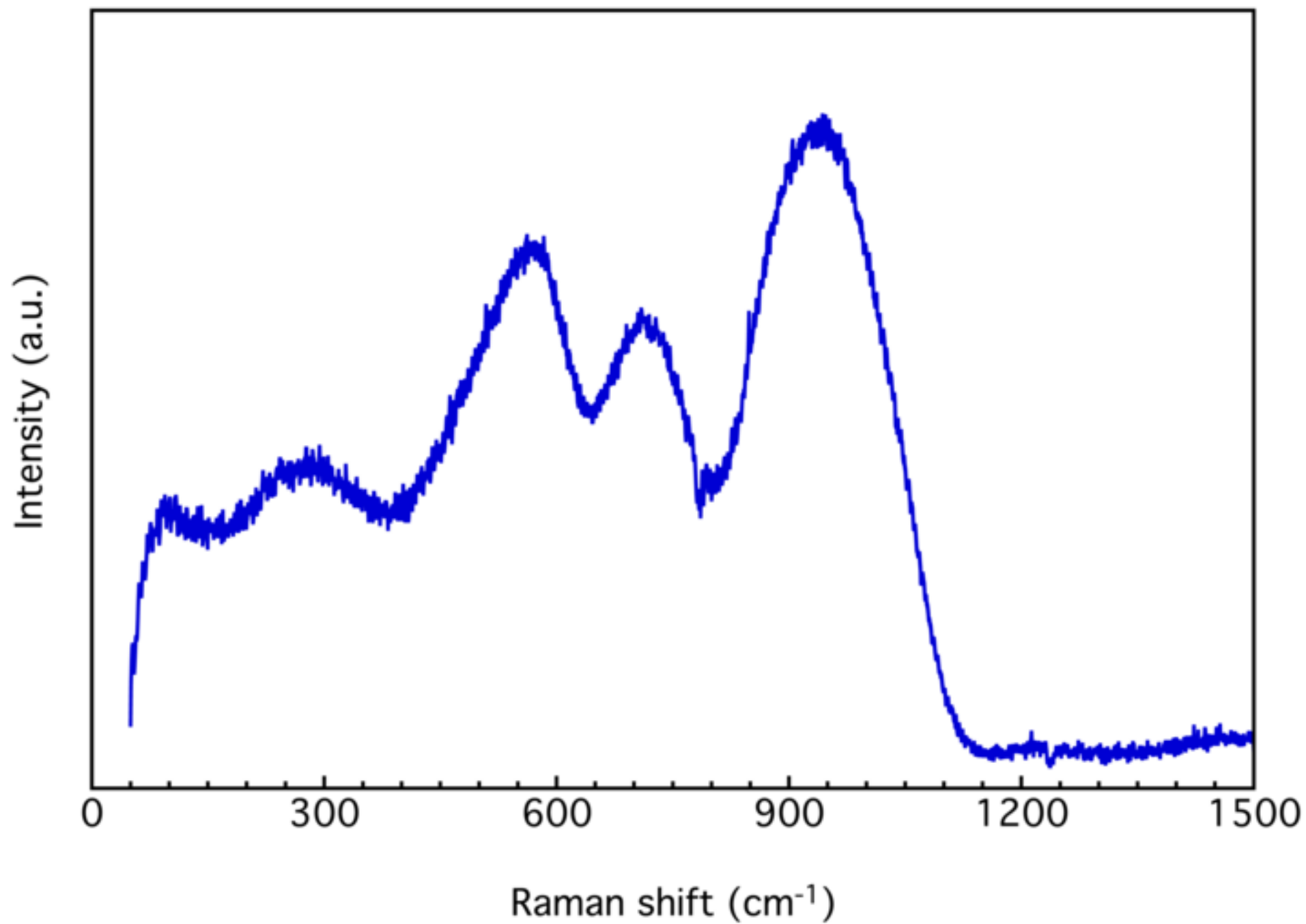


Figure 2
[Click here to download high resolution image](#)

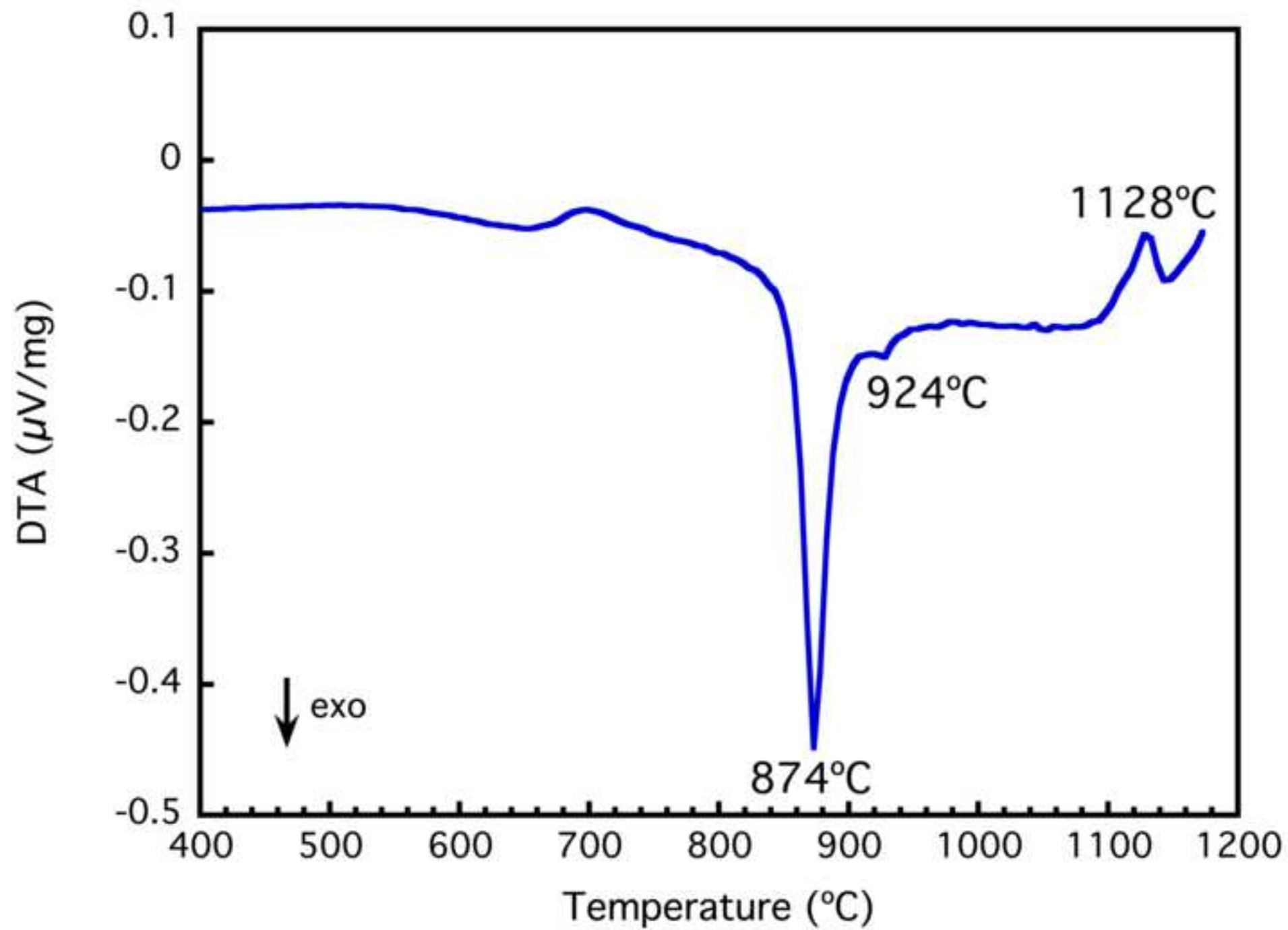


Figure 3
[Click here to download high resolution image](#)

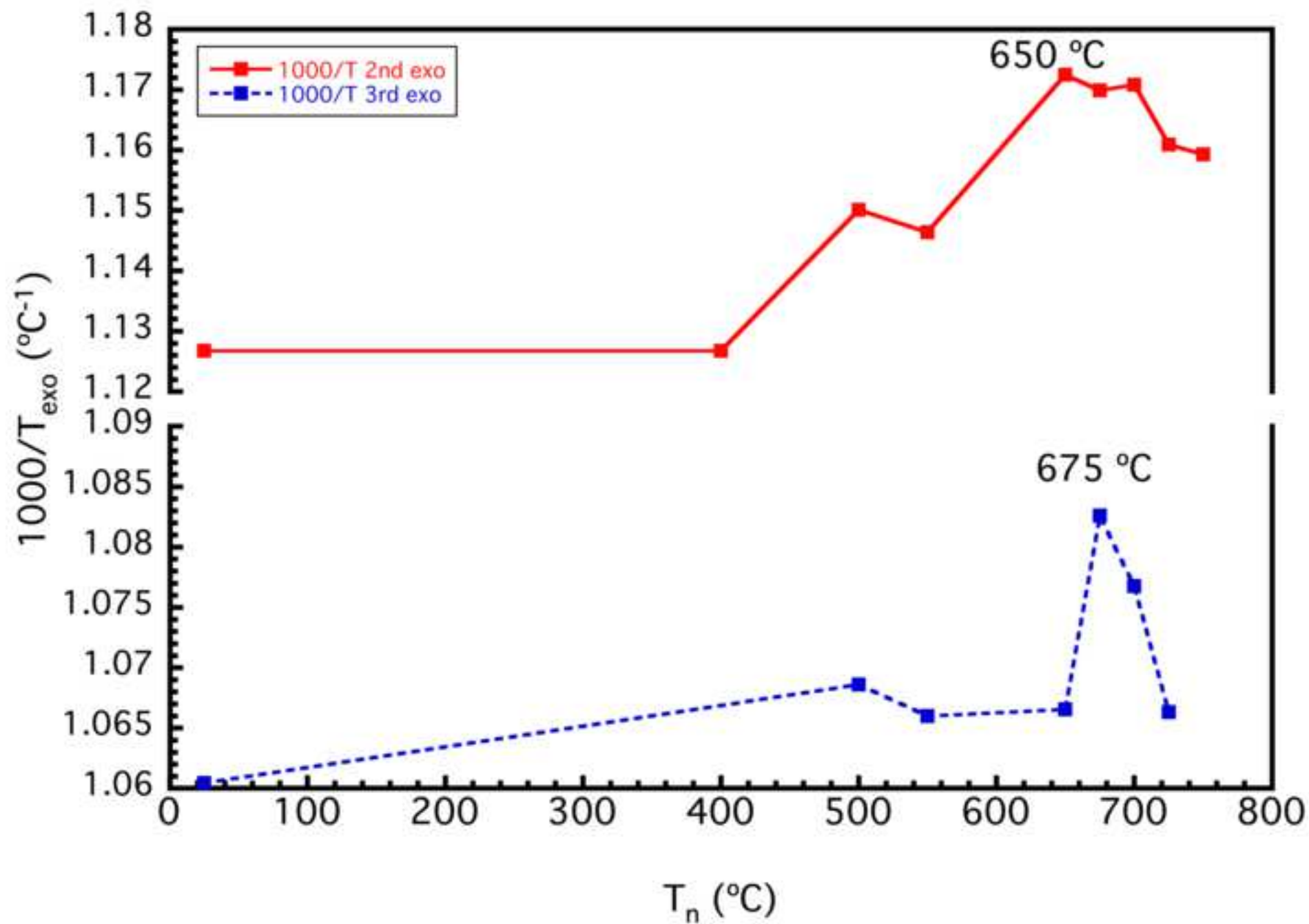


Figure 4

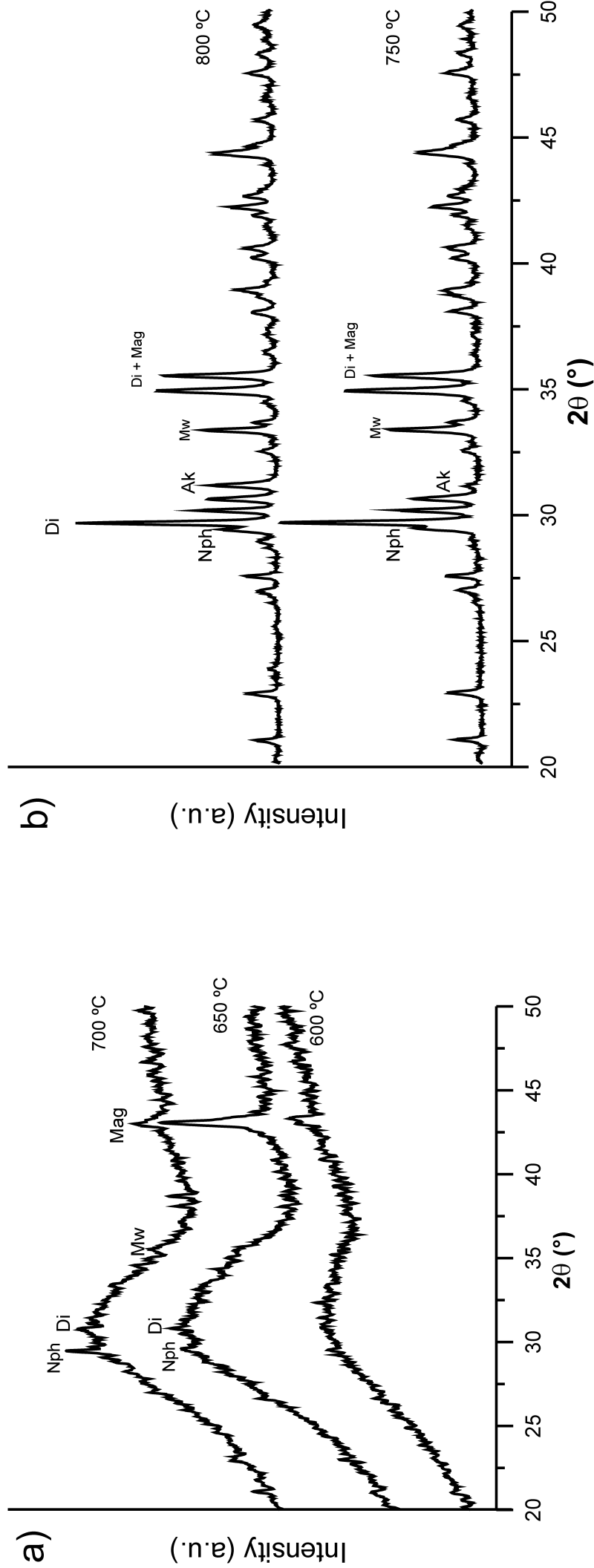


Figure 5
[Click here to download high resolution image](#)

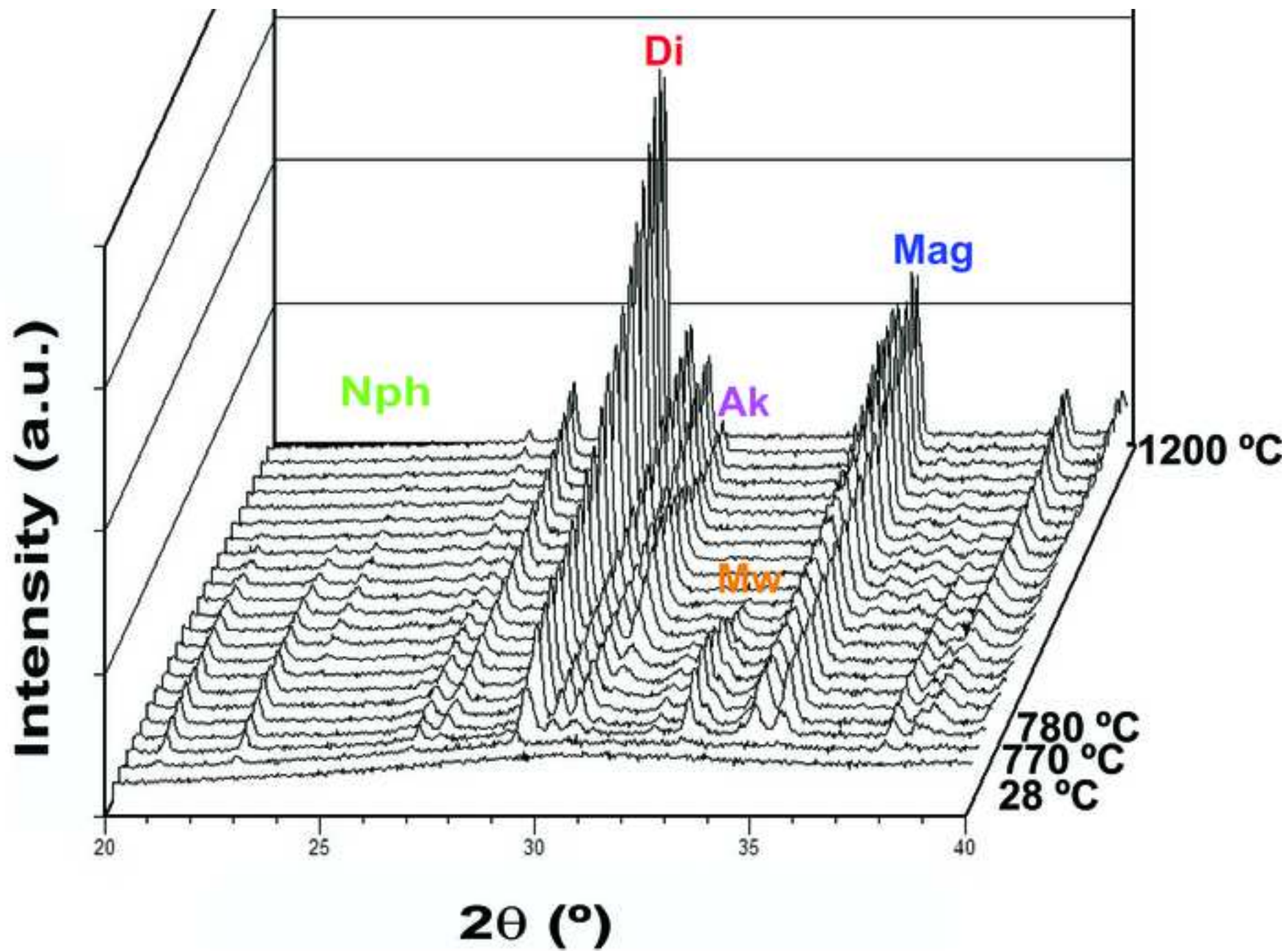


Figure 6
[Click here to download high resolution image](#)

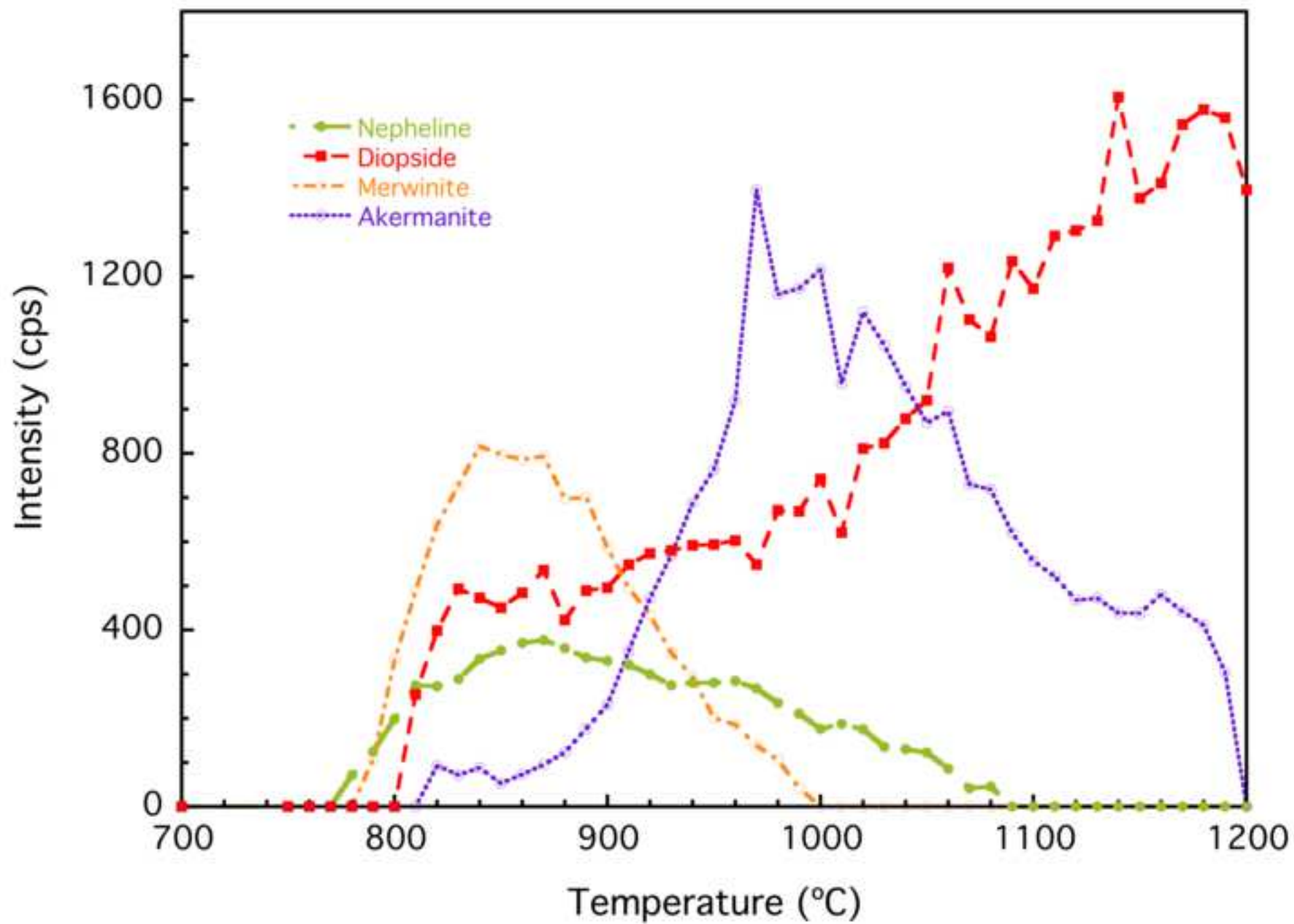


Figure 7

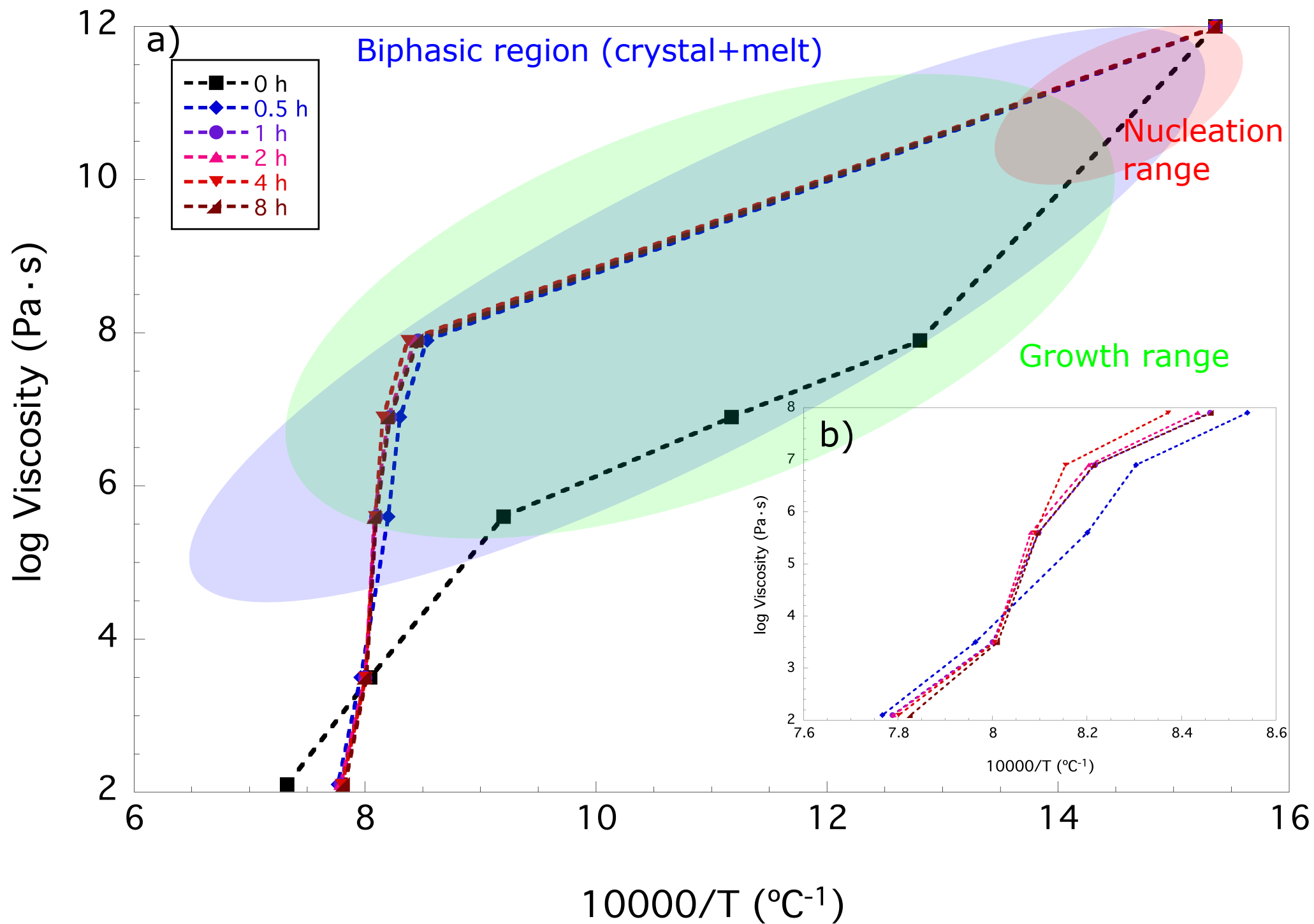


Figure 8
[Click here to download high resolution image](#)

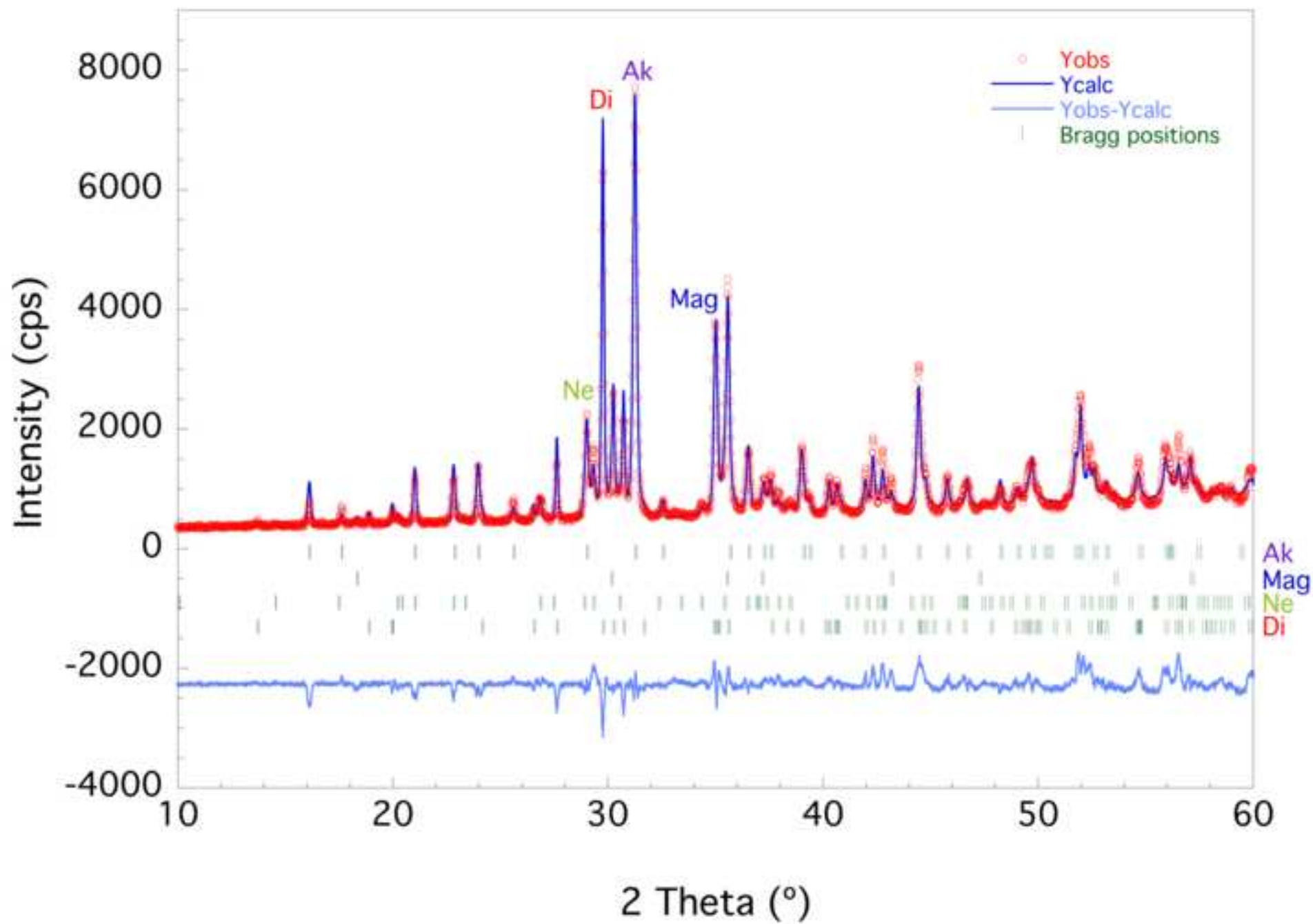


Figure 9
[Click here to download high resolution image](#)

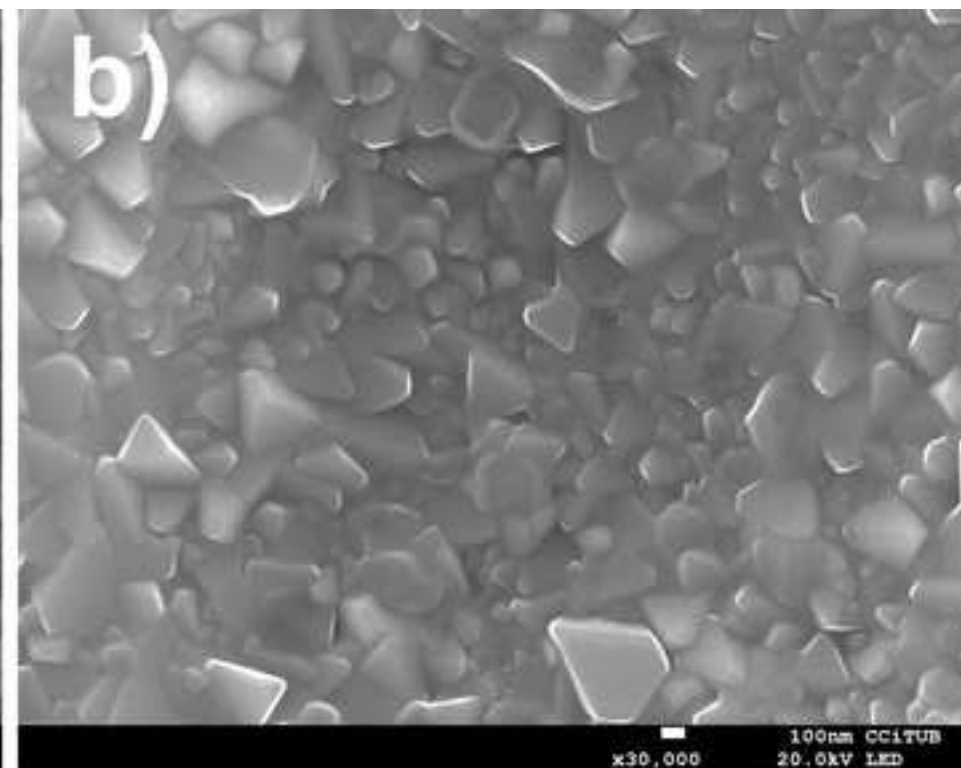
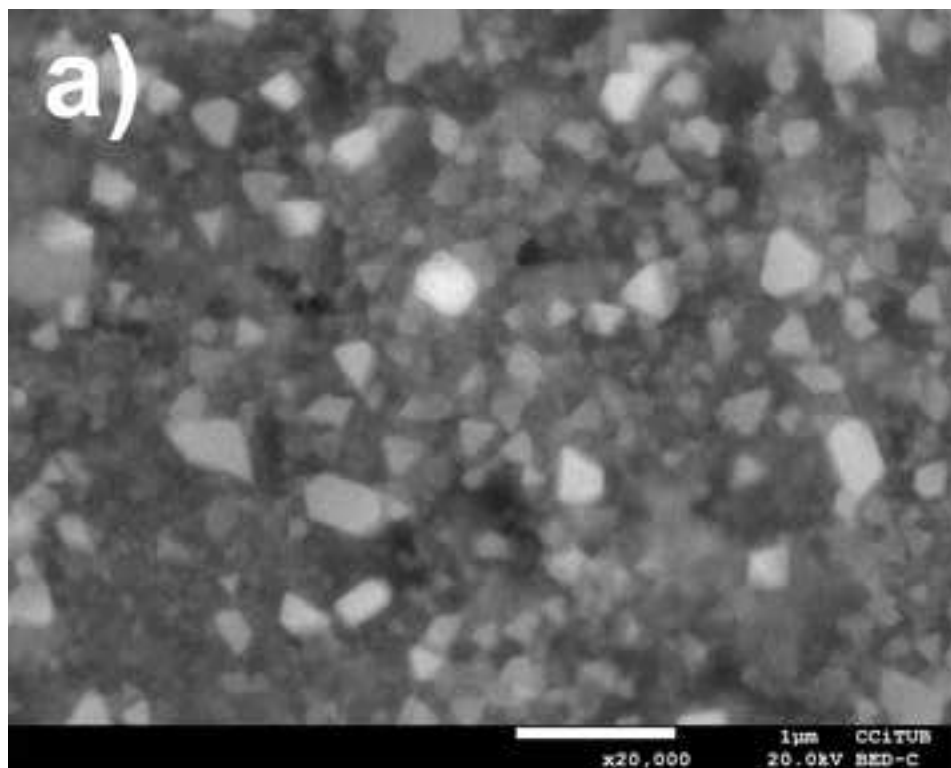


Table 1. Composition of the basalt from Sant Joan les Fonts compared to analysis of sewage sludge from WWTP available on the literature ([7,8,9-13]. The asterisks show the values which stray further from real sludge compositions.

Oxide	Basalt	USS compositions
Major components (wt%)		
SiO ₂	43.98	33 - 53.14
CaO	10.11*	7.7 - 37.67
Al ₂ O ₃	14.16	11.73 - 21.48
FeO	10.88	4.64 - 10
MgO	10.05*	2.4 - 6.52
Na ₂ O	3.31	0.6 - 5.2
TiO ₂	2.51	1.19 - 2.9
K ₂ O	1.98	0.9 - 3.8
P ₂ O ₅	0.55*	2.62 - 5.2
MnO	0.17	0.12 - 0.44
Trace elements (ppm)		
Ba	585.4	330
Cr	263.5	1268
Cu	63.6	12701
Ni	172.9	1025
Pb	4.9	3519
Zn	86.2	31166

Table 2. Chemical composition of the parent glass B16Ca obtained by EMPA.

wt%	SiO₂	Al₂O₃	Fe₂O₃	CaO	MgO	Na₂O	TiO₂	K₂O	P₂O₅	MnO
B16Ca _(glass)	36.11 (0.34)	12.19 (0.17)	10.06 (0.29)	24.44 (0.33)	9.19 (0.56)	2.28 (0.10)	2.02 (0.08)	1.12 (0.07)	0.46 (0.10)	0.15 (0.03)

Table 3. Intensities of the main diffraction peaks of the newly-formed mineral phases after sudden thermal treatments at the T_N followed by growth at the temperature of the first exothermic.

T_N (°C)	Newly-formed minerals (cps)				
	Magnetite	Nepheline	Diopside	Merwinite	Akermanite
600	113	-	-	-	-
650	301	63	431	-	-
700	165	167	265	-	-
750	-	1726	6001	2697	33
800	-	1450	5892	2218	1893

Table 4. Concentration of selected elements on the leachates after blank subtraction. BB stands for “below blank concentration” and BDL for “below detection limit”.

[ppm] in solution	Ca	K	Si	Na	Mg	Fe	Al	Ba	P
Glass	3.52	2.24	4.17	9.73	2.73	0.39	1.18	0.04	BB
Glass-ceramic	4.43	1.88	4.79	8.31	2.45	0.11	0.88	0.09	BB

[ppb] in solution	Zn	Pb	As	Cu	Cr	Ni	Cd	Ti
Glass	BB	0.83	0.23	11.09	BDL	9.00	BB	76.32
Glass-ceramic	2.85	1.04	0.71	10.68	BDL	7.16	0.18	26.73
DIN 38414-S4 [30]	4000	500	500	2000	500	400	40	N/A

Table 5. Microhardness results of this study compared to Vickers microhardness values for basaltic glasses and glass-ceramics in the literature.

Material	Vickers Microhardness (GPa)
Sant Joan les Fonts Basalt glass	7.7 ± 0.3
B16Ca glass	8.2 ± 0.5
B16Ca glass-ceramic	8.6 ± 0.5
Canary Island Basalt glass	5.16 – 6.28 [50]
Canary Island Basalt glass-ceramic	6.62 – 8.66 [50]
Basalt rock fiber glass	7.7 [51]
Basalt glass/crystal mixtures	6.8 – 8.9 [51]
Holyoke basalt glass	8.9 [52]